A West African Middle Stone Age site dated to the beginning of MIS 5: Archaeology, chronology, and paleoenvironment of the Ravin Blanc I (eastern Senegal)

Katja Douze, Laurent Lespez, Michel Rasse, Chantal Tribolo, Aline Garnier, Brice Lebrun, Norbert Mercier, Matar Ndiaye, Benoît Chevrier, Eric Huysecom

Journal of Human Evolution 154 (2021) 102952

Contents lists available at ScienceDirect

Journal of Human Evolution

journal homepage: www.elsevier.com/locate/jhevol

A West African Middle Stone Age site dated to the beginning of MIS 5: Archaeology, chronology, and paleoenvironment of the Ravin Blanc I (eastern Senegal)

Katja Douze [a, *], Laurent Lespez [b], Michel Rasse [c], Chantal Tribolo [d], Aline Garnier [b], Brice Lebrun [d], Norbert Mercier [d], Matar Ndiaye [e], Benoît Chevrier [a], Eric Huysecom [a]

[a] Laboratory of Archaeology and Population in Africa, Anthropology Unit, Department of Genetics and Evolution, University of Geneva, Quai Ernest-Ansermet 30, 1205 Genève, Switzerland
[b] Laboratory of Physical Geography (LGP), CNRS-UMR 8591, Department of Geography, University Paris-Est Creteil, 1 Place Aristide Briand, 920195 Meudon, France
[c] Laboratory Archéorient, CNRS-UMR 5133, Maison de L'Orient et de La Méditerranée, University of Lyon II, 7 Rue Raulin, 69007 Lyon, France
[d] Research Institute on Archaeological Materials-Centre of Research on Physics Applied to Archaeology (IRAMAT-CRP2A), CNRS-UMR 5060, University Bordeaux-Montaigne, Esplanade des Antilles, F-33607 Pessac Cedex, France
[e] Laboratory of Prehistory and Protohistory, Institut Fondamental D'Afrique Noire, University of Cheikh Anta Diop de Dakar, 33 Route de La Corniche Ouest, Dakar, Senegal

ARTICLE INFO

Article history:
Received 29 May 2020
Accepted 19 January 2021
Available online xxx

Keywords:
Lithic technology
Phytoliths
Optically stimulated luminescence
Geomorphology
Upper Pleistocene
Human behavior

ABSTRACT

The Ravin Blanc I archaeological occurrence, dated to MIS 5, provides unprecedented data on the Middle Stone Age (MSA) of West Africa since well-contextualized archaeological sites pre-dating MIS 4/3 are extremely rare for this region. The combined approach on geomorphology, phytolith analysis, and OSL date estimations offers a solid framework for the MSA industry comprised in the Ravin Blanc I sedimentary sequence. The paleoenvironmental reconstruction further emphasizes on the local effects of the global increase in moisture characterizing the beginning of the Upper Pleistocene as well as the later shift to more arid conditions. The lithic industry, comprised in the lower part of the sequence and dated to MIS 5e, shows core reduction sequences among which Levallois methods are minor, as well as an original tool-kit composition, among which pieces with single wide abrupt notches, side-scrapers made by inverse retouch, and a few large crudely shaped bifacial tools. The Ravin Blanc I assemblage has neither a chronologically equivalent site to serve comparisons nor a clear techno-typological correspondent in West Africa. However, the industry represents an early MSA technology that could either retain influences from the southern West African 'Sangoan' or show reminiscences of the preceding local Acheulean. A larger-scale assessment of behavioral dynamics at work at the transition period between the Middle to Upper Pleistocene is discussed in view of integrating this new site to the global perception of this important period in the MSA evolutionary trajectories.

1. Introduction

The West African Middle Stone Age (MSA) has attracted increasing attention over the past decade, while our knowledge of the region is among the lowest on the continent. Consequently, West Africa is currently not given much consideration in the evaluation of the human evolutionary history that takes place during this key period. Yet, this largely unknown region has the potential to enrich scenarios on the trajectories of emergence and development of *Homo sapiens* in Africa, as well as on the cultural and population movements of human groups. Culturally, an interesting scenario emerges with the very marked alternation of the types of MSA industries known for MIS 4/3 in Ounjougou, Mali, most likely reflecting a complex settlement history in the interior of West Africa during this period (Soriano et al., 2010; Chevrier et al., 2018). Conversely, cultural stability is argued for coastal occupations during the same period (Niang et al., 2020). New paradigms envisage considering West Africa at the crossroad between North

* Corresponding author.
E-mail address: Katja.Douze@unige.ch (K. Douze).

https://doi.org/10.1016/j.jhevol.2021.102952

Africa where the Mousterian and the Aterian have developed during the MSA (Scerri et al., 2016; Scerri, 2017) and Central Africa, which is known as being characterized by the Sangoan and Lupemban industries (Taylor, 2016). This crossroad zone would allow bypassing zones that are more arid by expanding across the Sudanian savannas and important hydrographic networks through the west coast (Niang et al., 2018). West Africa can alternately be seen as an area of population retrenchment, which would have affected the biological and cultural trajectory of the region's populations in a different way than in other parts of Africa (see Scerri et al., 2018 for the 'African multiregionalism' hypothesis). Most recent research further reinforces this vision of an original evolutionary scenario for West Africa, in which the MSA would have persisted until the Pleistocene to Holocene boundary, making it the youngest known MSA in Africa (Scerri et al., 2017, 2021).

However, regarding the period pre-dating MIS 4/3 usually assigned to the first developments of *H. sapiens* in Africa (e.g., McBrearty and Brooks, 2000), the lack of chronometric data in West Africa on well-stratified *in situ* archaeological sites is still a significant issue (Table 1). It hampers a comprehensive vision of the behavioral patterning for hominin populations at the end of the Middle Pleistocene and the beginnings of the Upper Pleistocene, which is a period of increasing human mobility and marked by an accelerated rate of innovation in several other regions of Africa (e.g., Groucutt et al., 2015; Porraz et al., 2013; Tryon and Faith, 2013; Wurz, 2013). Relative chronologies, usually based on climatic phases assessed from the sediments or on analogies with dated contexts from other regions (see synthesis of Allsworth-Jones, 2019), may indicate that this period in West Africa encompasses the end of the Acheulean and part of the MSA, often named 'Mousterian', based on the dominance of Levallois and discoid core reduction products (e.g., Corbeil et al., 1948; Descamps, 1979, Clark et al., 2008). The Aterian is recognized in the northern latitudes of West Africa, possibly starting during the course of MIS 5 (Clark et al., 2008:400), and pedunculated pieces were also mentioned in Senegal (e.g., Camara and Duboscq, 1987; Niang et al., 2018, 2020; Niang and Ndiaye, 2016; Scerri et al., 2016, 2017) but remain undated with the exception of Tiémassas (Table 1). In countries around the Gulf of Guinea, namely the Ivory Coast, Ghana, Nigeria, and Cameroun, the Sangoan has been identified as chronologically transitional between the Acheulean and the MSA. Its definition with regard to the Sangoan from Kalambo Falls where it was the best described (Clark et al., 2001) has been debated on numerous occasions (Soper, 1965; Davies, 1976; Nygaard and Talbot, 1984; Lioubine and Guede, 2000) and Andah (1979) even compared techno-typologically the Sangoan industry Sakumo I of Asokrochona (Ghana) to the Oldowan. A single absolute date obtained at the site of Bete I in Ivory Coast has, however, shown that the Sangoan was developed at the end of the Middle Pleistocene (Table 1), but the timing of the decline of the Sangoan corresponding to the emergence of the MSA is not yet defined.

In this context, we present a new site named the Ravin Blanc I, located in the Falémé River Valley, eastern Senegal, dated to the beginning of MIS 5, which has provided an original lithic industry that offers new insights into the beginnings of the MSA in West Africa. The site is currently the oldest well-dated and stratified assemblage of its kind in West Africa and has benefitted from a combined research work involving archaeology, geomorphology, geochronology, and phytoliths studies. These solid multidisciplinary data allow for the development of new hypotheses regarding the hominin evolutionary trajectories at work during the Middle to Upper Pleistocene transition in West Africa, in relation to the paleoenvironments, cultural patterning, and their chronology.

1.1. Site location and research background

The Ravin Blanc I site (13°59′5.04.2″ N, 12°13′23.3″ W) is located north from the village of Toumboura, in the Tambacounda Province, eastern Senegal (Fig. 1). It is situated in the lower valley of the Falémé river at an altitude of about 50 m asl. At around 1.5 km west of the Falémé in a straight line, a natural section containing an archaeological layer with a powdery-white appearance was found in 2016 and inspired the naming of the gully (Ravin Blanc meaning 'White Gully' in French). The site has been investigated in the framework of the international research program 'Human Population and Paleoenvironment in Africa', led by the University of Geneva. Since 2011, one of the research aims of this program is to document the Paleolithic chrono-cultural sequence of eastern Senegal (Lebrun et al., 2016, 2017; Chevrier et al., 2016, 2018, 2020; Rasse et al., 2020), following previous Paleolithic research by Camara and Duboscq led in the 1980s along the Falémé river (Camara and Duboscq, 1983, 1984, 1987, 1990).

1.2. Geomorphological setting

The Falémé, which is the main tributary of the Senegal River, rises in the Fouta Djalon at Mount Loura (1538 m) in Guinea and then flows northward into the Senegal River (Fig. 1). In the studied region, the Falémé defines a wide depression below the Manding plateaus and the Tambaoura escarpment to the east, and the Senegalese plateau, which dominates it immediately to the west (about 100 m asl). It cuts into the schisto-pelitic sedimentary Falémé series (Thévéniaut et al., 2010), encompassing in a rarely observable silt-clay basement, composed of centimetric to decimetric banks of various grauwackes, including banks of siliceous limestone and sandstone as well as fine green strata of jaspoid character (also known as silexite; Fig. 2). The eastern escarpment, located 3.5 km from the site, corresponds to a pseudo-cuesta armored by a lateritic crust developed in the Ordovician sandstones of the Boundou Group. The very flat topography of the depression corresponds to a polygenic glacis whose last phases of regradation are attributable to the Quaternary (Michel, 1973; Rasse et al., 2020). The most recent studies reveal almost continuous sedimentation over the last 100 ka along the Falémé (Davidoux et al., 2018; Rasse et al., 2020; Chevrier et al., 2020). It corresponds to alluvial and fluvio-aeolian formations, rich in archaeological remains (Chevrier et al., 2018). The Ravin Blanc gully is one of the many ravines on the left bank of the Falémé that progressively incises this surface, from a thickness of 1 m upstream to about 10 m at its confluence with the Falémé. The site is located about 5 km upstream of the confluence with the river if one follows the meandriform course of the ravine. There, the glacis is a combination of erosion revealing locally the most resistant banks of bedrock, grauwacke in particular, and accumulation corresponding to shallow Quaternary deposits. The recent incision in the ravine allows observing the Quaternary formations over a thickness of about 2 m, which have yielded the archaeological artifacts.

1.3. Environmental setting

The modern climate of the section of the Falémé River Valley under consideration is of tropical arid type (Köppen-Geiger climate type BSh; Kottek et al., 2006). The average rainfall is around 850 mm per year, distributed over the 5 months of the rainy season

Table 1
West African Sangoan and Middle Stone Age sites dated by absolute dating methods.

Country, area[a]	Site name	Stratigraphic	Dates (ka) associated with the archaeological occurrence				MIS	Technology	References
		Unit of the archaeological occurrence	Dates in bold are directly related to the archaeological occurrence. *Dates in italics are from the same site but from other stratigraphic units or from same stratigraphic units not directly related to the archaeological occurrence*					(Main attributes)	
Ivory Coast, Anyama quarries	Bete I	Layer D	*TPQ of 254 ± 51 from the lowermost level of layer D*				<8?	Unidirectional and discoidal cores, heavy and massive pick-like forms, bifacial tools, core-scrapers, choppers, side-scrapers, polyhedrals, on quartz of low quality. Qualified as Sangoan.	Paradis (1980); Lioubine and Guédé (2000)
Senegal, Falémé Valley	Ravin Blanc I	SU 1	**SU1: 128 ± 12** **SU1: 124 ± 12** *SU2:137 ± 17* *SU2 : 99 ± 12* *SU3:148 ± 15* *SU3 : 102 ± 10*				5	Algorithmic reduction, 'core-axes', pieces with large notches, end-scrapers few Levallois reduction, on sandstone	Douze et al., this study
			FMM Oxford	CAM Oxford	FMM Bordeaux	CAM Bordeaux			
Mali, Ounjougou	Kokolo 2	U2	*U2 : 62 ± 6*	*U2: 74 ± 8*	*U2: 69 ± 7*	*U2: 78 ± 8*	4	Assemblage of quartz pebbles similar to Oldowan-type industry, centripetal core reduction	Soriano (2003); Soriano et al. (2010); Tribolo et al. (2015)
					U2: 63 ± 6	*U2: 64 ± 7*			
				U2: 60 ± 5		**U2: 59 ± 6**			
			U5 : 37 ± 3	*U5: 35 ± 3*		*U5: 39 ± 4*			
			U5 : 30 ± 2	*U5: 29 ± 2*	*U5: 37 ± 4*	*U5: 30 ± 3*			
			U6 : 20 ± 2	*U5: 25 ± 2*	*U5: 20 ± 2*	*U5: 23 ± 2*			
Mali, Ounjougou	Oumounaama Atelier	U2	*U2: 62 ± 9*	*U2: 71 ± 11*			4	Two assemblages at same level:	Soriano et al. (2010); Tribolo et al. (2015); Chevrier et al. (2018)
			U2: 56 ± 6	**U2: 64 ± 7**				1) Blade production on sandstone cores	
			U4: 45 ± 5	*U4: 55 ± 6*				2) Bipolar-on-anvil and other	
Mali, Ounjougou	Oumounaama Ouest	U3?	*TAQ of U3: 63 ± 8*	*TAQ of U3: 52 ± 5*	*TAQ of U3: 45 ± 4*	*TAQ of U: 48 ± 5*	4/3?	Levallois on sandstone, bipolar-on-anvil on quartz and quartzite	Soriano et al. (2010); Tribolo et al. (2015)
			U3: 40 ± 3	*U3: 42 ± 4*		*U3: 42 ± 5*			
			U5: 29 ± 2	*U5: 30 ± 3*	*U5: 31 ± 3*	*U5: 36 ± 3*			
			U5: 32 ± 3	*U5: 32 ± 3*	*U5: 41 ± 3*	*U5: 41 ± 3*			
Mali, Ounjougou	Vipère 1, Lower and Upper	U3	**U3: 57 ± 5**	**U3: 55 ± 5**			4	Two assemblages, stratified: 1) Lower (U3): Discoid reduction on quartzitic sandstone 2) Upper (U3): Discoid on quartz	Soriano et al. (2010); Tribolo et al. (2015)
			U3: 52 ± 5	*U3: 42 ± 4*					
			U Hol: 7.8 ± 0.7	*U Hol: 10.2 ± 0.9*					
			U Hol: 6.0 ± 0.5	*U Hol: 7.3 ± 0.7*					
			U Hol: 6.5 ± 0.6	*U Hol: 6.7 ± 0.6*					
Mali, Ounjougou	Kondo	U3	**U3: 45 ± 5**	**U3: 59 ± 6**			4	Preliminary study: Bifacial foliate pieces, centripetal reduction	Tribolo et al. (2015); Chevrier et al. (2018)
Mali, Yawa	Songona 1	F3A				*F2: 77 ± 7* *F2: 71 ± 6* *F2: 69 ± 6* *F3A: 71 ± 6* *F3A: 51 ± 5* *F3A: 56 ± 5* *F3A: 56 ± 6* *F3A: 45 ± 4*	3	Bifacial foliates points on quartz and unidirectional algorithmic reduction strategy	Rasse et al. (2012); Chevrier et al. (2018)

(*continued on next page*)

Table 1 (*continued*)

Country, area[a]	Site name	Stratigraphic	Dates (ka) associated with the archaeological occurrence				MIS	Technology	References
		Unit of the archaeological occurrence	Dates in bold are directly related to the archaeological occurrence. *Dates in italics are from the same site but from other stratigraphic units or from same stratigraphic units not directly related to the archaeological occurrence*					(Main attributes)	
						F3A: 44 ± 4 **F3A: 40 ± 4** *HOL: 0.6 ± 0.3* *HOL: 0.7 ± 0.2*			
Mali, Ounjougou	Draperies	U5	**U5: 43 ± 5**	**U5: 43 ± 5**			3	Preliminary study: Bifacial pieces and shaping flake on surface and discoid reduction in stratigraphy	Soriano et al. (2010); Tribolo et al. (2015); Chevrier et al. (2018)
Mali, Ounjougou	Oumounaama butte	U6	**U6: 41 ± 6**	**U6 : 43 ± 6**			3	Preliminary study: Bifacial pieces and foliate points	Tribolo et al. (2015); Chevrier et al. (2018)
Mali, Ounjougou	Oumounaama Px	U5	**U5: 40 ± 3**	**U5: 40 ± 3**	**U5: 33 ± 3**	**U5: 39 ± 3**	3	Sandstone bifacial foliate points	Tribolo et al. (2015); Chevrier et al. (2018)
Mali, Ounjougou	Orosobo	U5	*U2: 55 ± 6* **U5: 44 ± 4**	*U2: 49 ± 4* **U5: 39 ± 3** *U5: 25 ± 2*	*U2: 42 ± 4* **U5: 45 ± 4**	*U2: 40 ± 5* **U5: 27 ± 3** *U5: 20 ± 2*	3	Discoid and centripetal Levallois reduction, scrapers, denticulates and retouched pseudo-Levallois points, on quartz, quartzite, and quarzitic sandstone	Soriano et al. (2010); Tribolo et al. (2015)
Mali, Ounjougou	Oumounaama Coupe Frank, Lower and upper	U3 U4	**U4: 43 ± 4** **U4: 37 ± 3**	**U3: 18 ± 2** **U4: 47 ± 4** **U4: 23 ± 3**	**U3: 41 ± 4** **U4: 37 ± 5**	**U3: 19 ± 3** **U4: 48 ± 6**	3	Two assemblages, stratified: 1) Lower (U3): discoid, bipolar-on-anvil on quartz, and unidirectional on sandstone 2) Upper (U4): discoid on quartz and quartzite	Soriano et al. (2010); Tribolo et al. (2015)
Mali, Ounjougou	Kokolo 3 c.3	U5	**U5: 31 ± 3** **U5: 33 ± 4** *U7: 17 ± 2*	**U5: 33 ± 3** **U5: 26 ± 3** *U7: 15 ± 2*			3	Sandstone bifacial points	Soriano et al. (2010); Tribolo et al. (2015)
Mali, Ounjougou	Dandoli 1 (also called Dandoli 1/3 and same archaea. Horizon as Dandoli 2)	U5	*U5: 33 ± 3* **U5: 30 ± 4** **U5: 36 ± 4** *U6: 28 ± 3* *U6: 23 ± 2* *U6: 18 ± 2*	*U5: 33 ± 3* **U5: 34 ± 4** **U5: 35 ± 4** *U6: 26 ± 3* *U6: 24 ± 2* *U6: 19 ± 2*			3	Bipolar-on-anvil on quartz and quartzite (same archaeological horizon as Dandoli 2)	Soriano et al. (2010); Tribolo et al. (2015)
Mali, Ounjougou	Dandoli 2 (same archaea. Horizon as Dandoli 1-1/3)	U5	**U5: 30 ± 3**	**U5: 30 ± 3**	**U5: 32 ± 3**		3	Sandstone heavy scrapers (same archaeological horizon as Dandoli 1−1/3)	Soriano et al. (2010); Tribolo et al. (2015)
Mali, Ounjougou	Sinkarma 1	U5	**U5: 34 ± 4**	**U5: 23 ± 3**			3	Sandstone heavy scrapers	Soriano et al. (2010); Tribolo et al. (2015)
Senegal, Western coast	Tiémassas	S7−S5	**S7: 61.9 ± 2.6** **S6: 47.3 ± 2.9** **S6: 43.8 ± 2.81** **S5: 25.9 ± 1.3** *S5: 2.16 ± 30* *S4: 2.87 ± 0.13* *S3: 1.73 ± 0.09*				4(?), 3, 2(?)	Opportunistic unipolar, multidirectional, unidirectional and centripetal Levallois cores, discoid flakes and cores, side-scrapers, denticulates, notches, rare bifacial retouching, limaces, tanged tools, on sandstone and chert.	Niang et al. (2018); 2020; Niang and Ndiaye (2016)
Senegal, Falémé Valley	Toumboura III	Uj	**Uj: 35 ± 3** **Uj: 33 ± 3** *Uj: 27 ± 2*				3	Bifacial pieces and foliate points, mainly on sandstone and chert	Lebrun et al. (2016); Chevrier et al. (2016); Lebrun (2018)

Table 1 (*continued*)

Country, area[a]	Site name	Stratigraphic	Dates (ka) associated with the archaeological occurrence	MIS	Technology	References
		Unit of the archaeological occurrence	Dates in bold are directly related to the archaeological occurrence. *Dates in italics are from the same site but from other stratigraphic units or from same stratigraphic units not directly related to the archaeological occurrence*		(Main attributes)	
Senegal, Falémé Valley	Missira III	Uj	*Uj: 47 ± 4* **Uj: 37 ± 4** *Uj: 21 ± 2*	3	Preliminary study: bipolar-on-anvil, bifacial pieces, discoid, scrapers	Lebrun (2018); Rasse et al. (2020)
Niger, Northeastern part	Bilma	Coarse sandstone	*TAQ of 33.4 ± 2.5 from overlying lacustrine sandstone*	3(?)	Preliminary study: Levallois dominated industry	Delibrias et al. (1974)
Ghana, Northern Region	Birimi, Lower and Upper	**Lower:** Layer 3 in MSA Profile **Upper:** 105 cm in Northern excavation unit 25S 81E	MSA profile: *Layer 3: 58.4 ± 15.3* **Layer 3: 40.8 ± 11.4** *Layer 2: 20.4 ± 3.4* *Layer 1: 4.13 ± 0.55* Northern excavation units: **105 cm: 23.6 ± 2.9** 49 cm*: 7.81 ± 0.6* 5 cm*: 3.07 ± 0.48* <*0.7* cm *0.38 ± 0.06*	3	Two occurrences, stratified 1) Lower: one patinated mudstone blade. 2) Upper: patinated siltstone flakes Qualified as 'Ultimate Middle Stone Age'.	Hawkins et al. (1996); Casey et al. (1997); Quickert et al. (2003)
Senegal, Gambia river	Laminia	1B	*1A: 24.6 ± 0.98* **1B: 22 ± 0.85** **1B: 20.8 ± 0.83**	1	Excavated material and surface collection: Preferential Levallois cores, few single platform and multiplatform cores and tested pebbles, flakes, on quartz and few on quartzite	Scerri et al. (2021)
Senegal, Faleme river	Saxomununya	Surface	*TPQ* of 11.1 ± 0.58 on terrasse deposits used as raw material source	1	Excavated material and surface collection: Preferential Levallois cores, single platform, multiplatform, amorphous and discoid cores, Levallois flakes, denticulates, side and end scrapers, notches, small foliate points, on quartz and few on quartzite	Scerri et al. (2021)

All open air sites. For the Ounjougou data, several ages are displayed for each sample, since the dating was performed with slightly different methods either in Oxford and/or in Bordeaux and two statistical models were applied to the equivalent dose distributions, either the finite mixture model (FMM), or the Central Age Model (CAM; Tribolo et al., 2015). Most of the time, they give consistent ages. *TPQ: terminus post quem; TAQ: terminus ante quem.*

[a] West African countries considered here comprise Benin, Burkina Faso, Cape Verde, The Gambia, Ghana, Guinea, Guinea-Bissau, Ivory Coast, Liberia, Mali, Mauritania, Niger, Nigeria, Senegal, Sierra Leone and Togo.

(June–October), corresponding to the Sudanian climate of West Africa. This seasonality is the result of the northward displacement of the monsoon. Consequently, the Ravin Blanc gully is only traversed by temporary runoff during the rainy season.

The current landscape of the region corresponds to a Sahelo-Sudanian wooded savanna (White, 1983). However, at the site's scale, we identify a mosaic of vegetation typical of wooded savanna, shrubby savanna, and gallery forest along the watercourses and ravines. The tree species depend on the soil type, the topography, and the water availability. The glacis surrounding the site are covered by a vegetation characterized by species such as *Acacia seyal*, *Balanites aegyptiaca, Ziziphus mauritania*, *Guiera senegalensis, Piliostigma reticulum,* and *Combretum* spp. while the gallery forest is composed of *Acacia nilotica*, *Acacia ataxacantha,* and *Diospyros mespiliformis.* The current landscape is strongly altered by human activity (e.g., pastoralism, agriculture, fire). The main cultivated species are pearl millet (*Pennisetum glaucum*), sorghum (*Sorghum bicolor*), maize (*Zea mays*), or groundnuts (*Arachis hypogaea*).

2. Materials and methods

2.1. Archaeology

In 2016, a first test-pit allowed collecting dating material for OSL analyses, paleoenvironmental reconstructions through thin sections and phytolith analyses, as well as lithic material for a first techno-typological diagnosis (Huysecom et al., 2017). In 2017, the test-pit was enlarged to collect a larger sample of archaeological material and for a better understanding of the deposition dynamics of the sediments. The main excavation area extends on a surface of 4 sqm in a form of a trench, oriented perpendicular to the natural section of the gully, toward the center of the riverbed (Fig. 3). The excavations were organized following arbitrary spits of 10 cm in which material was collected by 1/4 sqm. Sedimentary texture for each spit was described throughout. All sediments were sieved with a 0.5-mm mesh.

The lithic material presented in this article was collected from the two main stratigraphic units (hereafter: SU) at the base of the

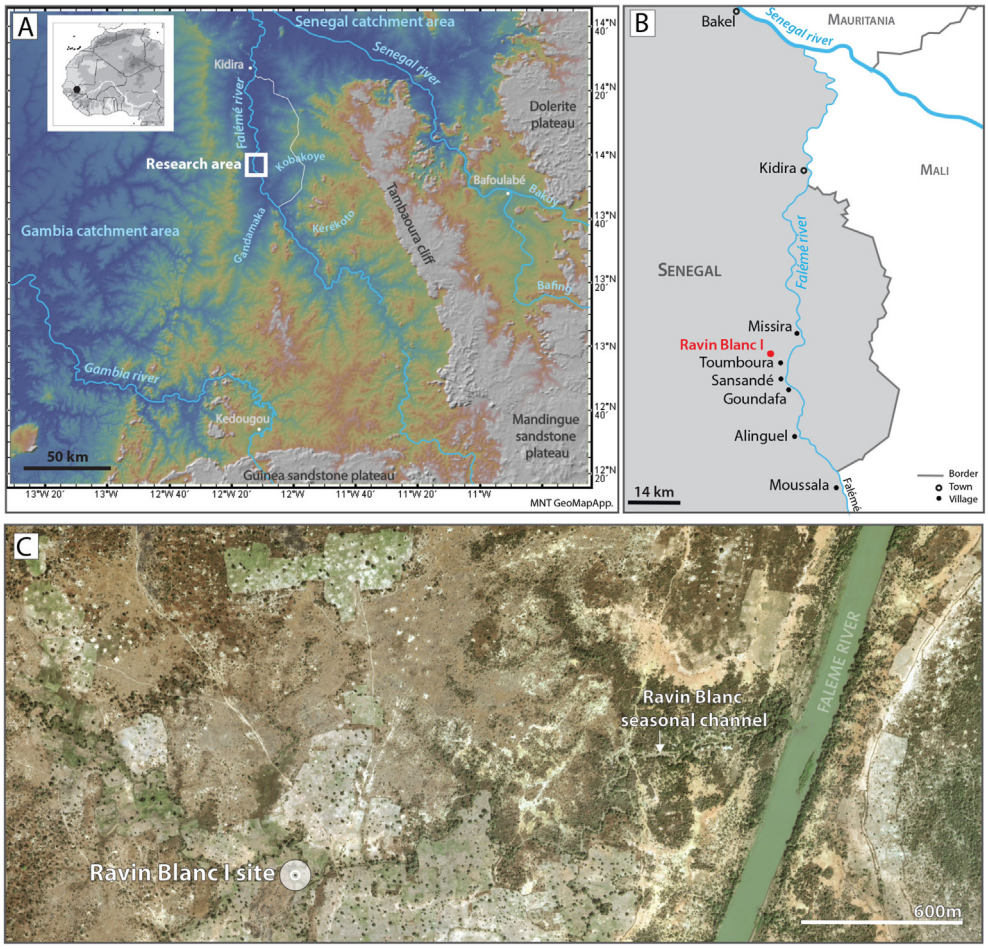

Figure 1. Location of the research area and the Ravin Blanc I site. A: Topography and hydrology of the region of research. B: Location of the site with regards to local villages. C: Location of the site with regards to the Falémé river (satellite image by Google Earth). (For interpretation of the references to color in this figure legend, the reader is referred to the Web version of this article.)

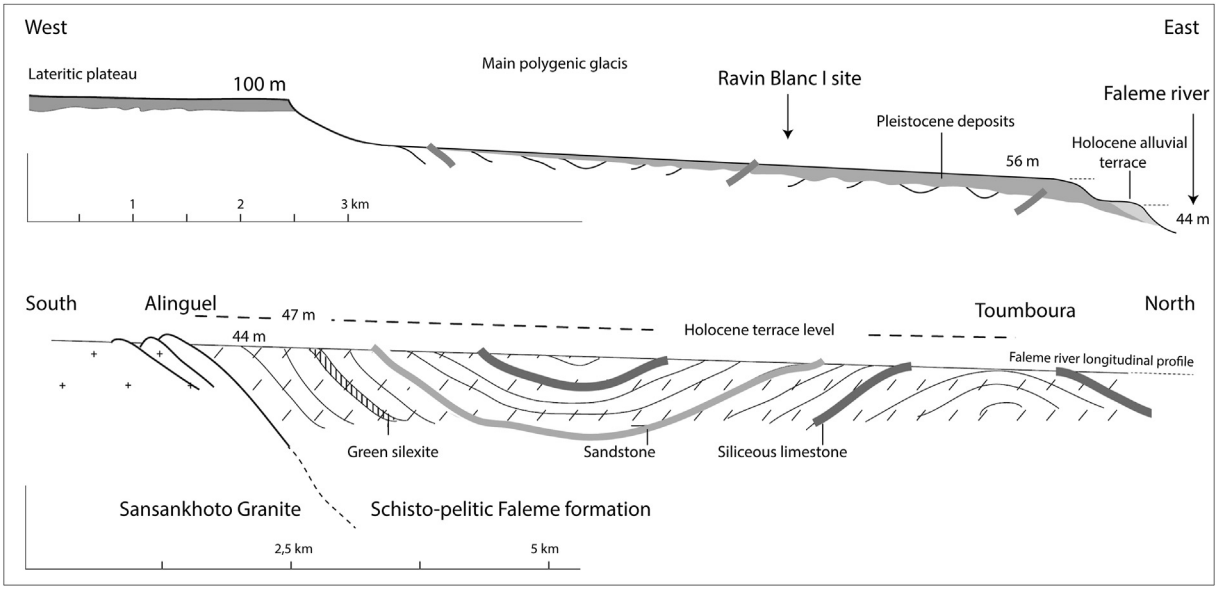

Figure 2. Schematic view of the geologic and geomorphologic context of the Ravin Blanc I site. Upper view: transversal West–East profile. Lower view: longitudinal upstream–downstream profile along the Falémé river.

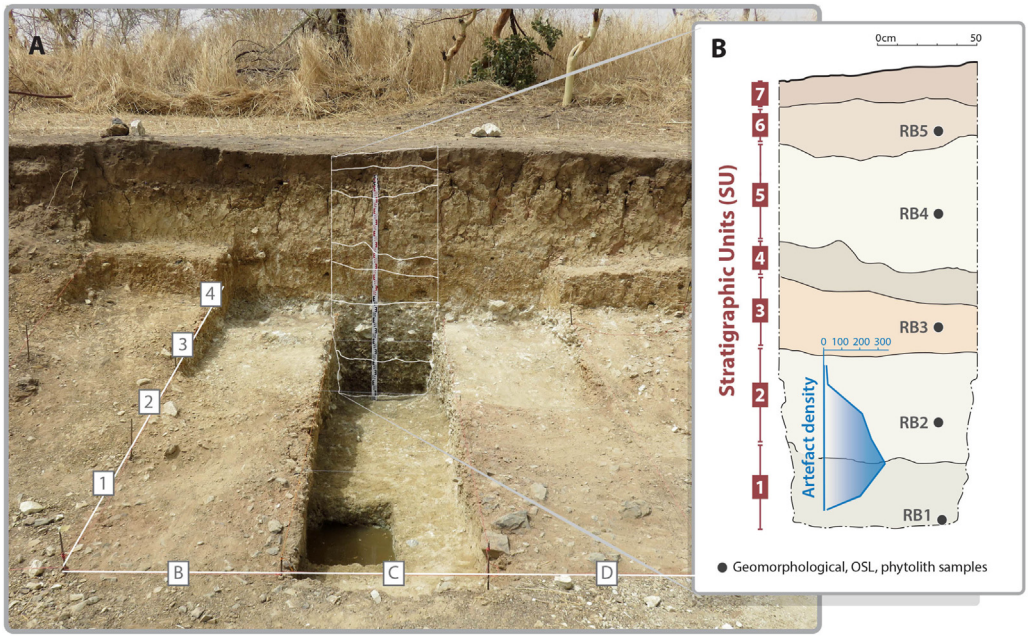

Figure 3. Excavation area and stratigraphy at the Ravin Blanc I site. A: View on the excavation area and excavation grid. B: Stratigraphic units, location of samples, and artifact density. (For interpretation of the references to color in this figure legend, the reader is referred to the Web version of this article.)

sequence, SU1 and SU2, which are securely documented in terms of geomorphology. A total of 1136 lithics was considered, of which 6.5% result from the 2016 test excavations, and 93.5% was collected during the extended excavations led in 2017. The assemblage originates from two adjoining squares: C3 and C4. These two squares were excavated in the slope down to the sterile basal layer in the maximum thickness of SU1 and SU2 deposits, reaching ca. 1m in C4 toward the section and ca. 0.8 m in C3. These squares contain 81% (n = 1136/1407) of the total amount of material collected at the Ravin Blanc I site. The rest of the material was not taken into account, either because of the recent dates obtained from the SU in which it was found or because of its unreliable depositional history, in particular toward the center of the current river bed.

The lithic study was performed following common standards of technological and typological analyses on all the lithics, without size discrimination. The study provides for a diagnosis of the main characteristics of the core reduction strategies combined with the characteristics of the end-products as well as a description of the main formal tool classes. To clarify a few important terms used in the lithic descriptions, 'end-product' designates a lithic product (flake or blade) that has a balanced morphology, peripheral cutting edges, and bears no or very few ($\leq$5%) cortical surfaces. It was supposedly produced in an advanced stage of the core reduction, after an operational sequence that aimed at preparing the core surfaces and managing convexities, knapping platforms as well as guiding ridges. 'Core management' products are lithic products (flakes or blades) that result from the latter, often bearing extended cortical planes (>5%), irregular peripheral morphologies and unbalanced morphologies. 'First flakes' are 100% cortical, although the choice was made to include in this group the products with non- or semi-cortical platforms. 'Centripetal,' 'unidirectional,' and 'bidirectional' refer to the direction of the negative scars on the dorsal face of the lithic products. Finally, a 'blank' designates a lithic artifact that has been used as a matrix to manufacture a formal tool (i.e., often a flake or a blade but could also be a pebble) or to lead a core reduction sequence (i.e., either a flake or a natural rock).

Retouch has been recorded following the analytical grid suggested by Inizan et al. (1999), including retouch position (direct, inverse/ventral, combined direct-inverse), their extent with respect to the center the piece in the axis perpendicular to the length (short: 1/4, medium: 2/4, invasive: 3/4 covering: 4/4), retouch inclination (abrupt: 90–71°, semi-abrupt: 70–40°, low-angled: <40°), their morphology (scaled, subparallel, Clactonian), and retouched edge delineation (straight, concave, convex, denticulated).

2.2. Geomorphology

The geomorphological investigations were carried out by the description of cross-sections in Pleistocene formations revealed by the Holocene incisions. These enabled the stratigraphy of the superficial formations of the Ravin Blanc to be established and to define the stratigraphic position for the archaeological remains. At the same time, examination of the sediments allowed highlighting the succession of sedimentary facies and to take samples for laboratory analyses. At the level of each OSL sampling, sediments were sampled in bulk for granulometric and phytolithic analyses. At the same level, blocks of sediment were collected for micromorphological analyses. The sampled blocks were wrapped in plaster strips to preserve the structure of the sediment. They were then impregnated and reduced to large thin strips (12 × 6 cm) using conventional methods (Guilloré, 1980). A total of five thin sections were taken from above (RB3, RB4, RB5), below (RB1), and within the archaeological horizon (RB2; Fig. 3). They were examined with a petrographic microscope according to the methods proposed by Bullock et al. (1985). Micromorphological analyses were used to detect the organization of sedimentary microfacies and soil features (humification, biological activity, micro-aggregation, hydromorphic features, calcitic, oxidation, and desiccation features).

2.3. Phytolith analyses

Phytolith assemblages have been analyzed for four samples (RB1–RB4). Phytolith extraction has been conducted on dried

samples of 30 g and treated through standard procedures: 1) destruction of organic matter with hydrogen peroxide (H_2O_2 33%, at 90 °C); 2) clays deflocculation with sodium hexametaphosphate (40 g/L); 3) sands removal by sieving at 250 μm and clay removal by decantation; and 4) densiometric separation with zinc bromide heavy liquid ($ZnBr_2$) set at d = 2.3. Immersion oil was used as mounting medium to allow 3D observations. Phytoliths were counted at 400× and 630× magnification. Absolute phytolith counts range from 205 to 319 diagnostic morphotypes depending on phytolith concentration and corrosion.

Phytolith morphotype classification and description are based on the ICPN 2.0 classification (ICPT: Neumann et al., 2019) and information from the literature (see Table 2 for references). Diagnostic morphotypes were classified into four main categories (Table 2). First, woody dicotyledons are represented by four main morphotypes. The POLYHEDRAL to CYLINDRICAL FACETATE morphotype is a characteristic of woody dicotyledons sclereids (Runge, 1999; Neumann et al., 2009; Garnier et al., 2013, 2018). The NODULAR and GRANULAR silica bodies have been identified by Collura and Neumann (2017) in modern West African wood. The SPHEROID ORNATE phytolith is more ubiquist and characteristic of woody dicots. This type encompasses spheroidal phytoliths with a wide range of ornamentation and shapes (Neumann et al., 2019). Despite their low taxonomic information, we distinguished in our study three subtypes according to their ornamentation (verrucate, baculate to pilate and tuberculate; Table 2).

Second, Arecaceae (palms) are characterized by a specific morphotype: SPHEROID ECHINATE. In our studied area, palms have mainly been observed in the gallery forests of the Falémé Valley, but they remain sparse.

Third, the Poaceae category is illustrated by grass silica short cell phytoliths (GSSCPs) produced in the epidermis of Poaceae. Some studies conducted on the GSSCP produced by West African grasses have focused on the micromorphological features of these short cells and especially of bilobates (length/width of the base, shank, and lobes or shape of outer margins). These studies pointed the need to use a finer classification to improve taxonomic resolution and paleoecological reconstructions (Fahmy, 2008; Novello et al., 2015; Neumann et al., 2017; Bourel and Novello, 2020). In this study, we chose to follow the classification from Neumann et al. (2017) based on 51 common grass species of West Africa that produced a standardized method for the identification of 20 supertype classes of GSSCP, from which 16 have been observed in the current study (Supplementary Online Material [SOM] Table S1). BILOBATE and CROSSES are mainly produced by Panicoideae. In this study, eight subtypes of BILOBATES and three subtypes of CROSSES have been differentiated according the size of the particle and the length of the shank. SADDLE are mainly produced by Chloridoideae while RONDEL are redundant with Poaceae. Finally, the herb category is illustrated by some specific morphotypes that can be related to the monocotyledons' family such as Commelinaceae and Cypercaeae. The POLYGONAL SCROBICULATE with cone is mainly produced by the Cyperaceae (Ollendorf, 1992) and in particular the *Cyperus* genus (Murungi and Bamford, 2020) which is specific to wetlands, but some species are also found in fields on the interfluves (Le Bourgeois and Merlier, 1995). Two other morphotypes (POLYGONAL DENTATE with top concave conical and PRISMATIC upper part psilate, basal part scrobiculate) have been identified by Eichhorn and colleagues (2010) as being produced by the Commelinaceae. These herbaceous species occur in West Africa, either in wetlands or anthropogenic environments (*Commelina* sp.) or on sandstone crusts (*Cyanotis lanata*). The morphotype BULLIFORM FLABELLATE are epidermal cells that occur both in Poaceae and Cyperaceae (Metcalfe, 1960, 1971; Esau, 1965) while PAPILLATE are known from grasses, specifically grass inflorescences (Piperno, 2006).

Non-diagnostic morphotypes were also identified and counted. Apart from this general approach, we applied the calculation of the D/P index to evaluate the tree cover density (Alexandre et al., 1997). The calculation is the ratio of SPHEROID ORNATE phytoliths (dicotyledons) versus total GSSCP (Poaceae). Values higher than 1 suggest a forest vegetation while values lower than 1 indicate an open environment.

2.4. Optically stimulated luminescence dating method

Five sediment samples (RB1–RB5) have been taken for being dated with the optically stimulated luminescence dating method (OSL; Aitken, 1985), together with the geomorphological and phytolith samples (Fig. 3). The sample were taken at night under subdued orange light, after the surface previously exposed to daylight has been scratched and discarded.

Samples were prepared following standard procedures to extract 200–250 and 100–140 μm quartz grains: wet sieving, followed by HCl (10%), then H_2O_2 (30%) to remove carbonates and organic material respectively. High-density liquid separation was performed using heteropolytungstate of sodium at 2.72 and 2.62 g/cm^3 to separate quartz, feldspars, and heavy minerals, although very few feldspar grains were available in the 100–140 or 200–250 μm fractions. The quartz grains were submitted to an HF (38%) etching for 60 min followed by a HCl treatment and a final sieve at 80 μm or 180 μm. The quartz then was mounted on single grain discs, presenting 100 holes with diameter 150 μm and 150 μm depth (RB1, RB4, RB5) or 300 μm diameter and 300 μm depth (RB2 and RB3) so that there was only one grain per hole. Multigrain discs (5-mm mask) were also prepared for preliminary tests.

Measurements were performed with a Risoe TL/DA 20 reader (Bøtter-Jensen et al., 2003), with single-grain green stimulation (10 mW Nd:YVO_4 diode-pumped laser at 532 nm) and detection in the UV wavelength range (280–380 nm obtained with 7.5 mm of Hoya U340 filters in front of a Q9235 photomultiplier tube). A calibrated beta source delivering 0.11 Gy/s was attached to the reader. The luminescence data were analyzed using Analyst v. 4.57 (Duller, 2015). Growth curves were fitted with a single saturating exponential [$Lx/Tx = a\,(1 - \exp((-(D + b)/D_0)))$], where Lx is the signal for the regenerative dose D, Tx is the signal for the following test dose, a, b, and D_0 are the fitting parameters.

Preliminary tests included linearly modulated OSL measurements (LM-OSL) and infrared-stimulated luminescence (IRSL) measurements, following Duller (2003). The IRSL tests showed that the quartz samples were not contaminated by any remaining feldspar grains. The LM-OSL test (SOM Fig. S1) showed that the signal was dominated by a fast component, which is a necessary condition for applying the single-aliquot regenerative-dose protocol (SAR; Murray and Wintle, 2000, 2003; Wintle and Murray, 2006). The SAR protocol (see SOM Fig. S2) then was tested on each sample: after bleaching in a solar simulator, a known beta dose was given in the reader, and the protocol was applied with a 260 °C 10 s preheat (natural and regenerative dose) and a 160 °C cut heat (test dose preheat). The dose to recover was chosen close to the equivalent dose estimated in preliminary runs for each sample. Grains were selected based on their sensitivity (natural test dose signal higher than three times background, and natural test dose relative error lower than 10%), the absence of any significant charge transfer (recuperation ratio <5% of maximal regenerative dose signal), and the success of the correction for sensitivity changes (recycling ratio <10%). A fair number of grains while passing these criteria were rejected because the natural signal was apparently beyond the saturation limit (see Table 3). The central age (actual dose) model was applied (Galbraith et al., 1999). The central dose was calculated while progressively discarding the grains with the

Table 2
Phytolith morphotype classification used in the study of the Ravin Blanc I site.

Plant group interpretation	Name (after ICPN 2.0[a])	CODE (after ICPN 2.0)	Description	Size (μm)	Anatomical origin[b]	References
Woody dicotyledons	POLYHEDRAL to CYLINDRICAL FACETATE	POL_FACE	Polyhedral to cylindrical shape having distinctive large flat or concave faces	20–200	Sclereids or terminal tracheid in L of woody dicotyledons	Postek (1981); Piperno (2006); Runge (1999) (A4; C2 and C3); Neumann et al. (2009); Garnier et al. (2013)
	SPHEROID ORNATE	SPH_ORN	Spheroidal to ellipsoid solid phytoliths with various ornamentations, single or composed	3–30	L, W, F of woody dicotyledons	E.g., ICPT: Neumann et al. (2019)
	NODULAR	NOD	Aggregation of small, smooth nodules with various shapes (globular, elongate, irregular)	10–50	W of certain dicotyledons	Collura and Neumann (2017)
	GRANULATE	GRAL	Irregular aggregation of small, smooth granules	10–30	W of certain dicotyledons	Collura and Neumann (2017)
Palms (Arecaceae)	SPHEROID ECHINATE	SPH_ECH	Solid spheroidal to slightly ellipsoidal phytoliths with conical projections distributed over the entire surface	5–25	L,W, R of Arecaceae	e.g., ICPT: Neumann et al. (2019)
Grasses and herbs						
Mesophytic to xerophytic grasses	BILOBATE VLL/LS	BIL_2	Bilobate with very long length and long shanks	>26 (4–7)	Mainly in L,I of Aristidoideae, Panicoideae	Neumann et al. (2017)
Mesophytic to aquatic grasses	BILOBATE LL/VLS	BIL_3	Bilobate with long length and very long shanks	18–26 (>7)	Mainly in L,I of Panicoideae	Neumann et al. (2017)
Mesophytic to xerophytic grasses	BILOBATE LL/LS	BIL_4	Bilobate with long length and long shanks	18–26 (4–7)	Mainly in L,I of Panicoideae	Neumann et al. (2017)
Mesophytic to aquatic grasses	BILOBATE LL/SS	BIL_5	Bilobate with long length and small shanks	18–26 (<4)	Mainly in L,I of Panicoideae	Neumann et al. (2017)
Mesophytic to xerophytic grasses	BILOBATE ML/LS	BIL_7	Bilobate with medium-long length and long shanks	10–18 (4–7)	Mainly in L,I of Panicoideae	Neumann et al. (2017)
Mesophytic to aquatic grasses	BILOBATE ML/SS	BIL_8	Bilobate with medium-long length and small shanks	10–18 (<4)	Mainly in L,I of Panicoideae	Neumann et al. (2017)
Mesophytic to aquatic grasses	BILOBATE ML/CON	BIL_9	Bilobate with middle-long length and constriction of the shanks	10–18	Mainly in L,I of Panicoideae	Neumann et al. (2017)
Mesophytic to xerophytic grasses	BILOBATE SL/CON	BIL_10	Bilobate with small length and constriction of the shanks	7–10	Mainly in L,I of Panicoideae	Neumann et al. (2017)
Mesophytic to aquatic grasses	CROSS LL	CRO_2	Cross with long length	18–26	Mainly in L,I of Panicoideae	Neumann et al. (2017)
Mesophytic to aquatic grasses	CROSS ML	CRO_3	Cross with medium-long length	10–18	Mainly in L,I of Panicoideae	Neumann et al. (2017)
Mesophytic to aquatic grasses	CROSS SL	CRO_4	Cross with small length	7–10	Mainly in L,I of Panicoideae	Neumann et al. (2017)
Mesophytic to aquatic grasses	TRIANGLE CROSS	TRG_CRO	Three lobes arranged in a triangular shape	8–18	In L, I of all grasses	Radomski and Neumann (2011)
Mesophytic to xerophytic grasses	SADDLE	SAD	Saddle	8–20	Mainly in L,I of Chloridoideae	Neumann et al. (2017)
No ecological assignment	RONDEL	RON	Base rounded, top conical or keeled	6–20	In L, I of all grasses	Neumann et al. (2017)
No ecological assignment	OTHERS	GSSCP_OTH	GSSCP that cannot be clearly classified in a specific variant	5–20	In L, I of all grasses	Garnier et al. (2013)
Grasses and herbs	BULLIFORM FLABELLATE	BUL_FLA	Fan-shaped morphotype	40–200	L of Poaceae and Cyperaceae	E.g., ICPT: Neumann et al. (2019)
Grasses and herbs	PAPILLAE	PAP	Elongated to circulate-oval plate having one or more short, conical, blunt or pointy protrusions (apex)	10–40	Mainly in I of Poaceae	E.g., ICPT: Neumann et al. (2019)
Herbs — Cyperaceae	POLYGONAL SCROBICULATE with cone	POL_1	Polygonal shape with scrobiculate ornamentation and entire margins having one short, conical or blunt protrusion (apex) in the center	15–35	L of Cyperaceae	Ollendorf (1992); Runge (1999); Strömberg (2004); Albert et al. (2006); Barboni et al. (2007); Neumann et al. (2009)
Herbs — Commelinaceae	POLYGONAL DENTATE with top concave conical	POL_2	Polygonal shape, psilate, slightly convex margin dentate, bent upward; upper part conical, lateral walls concave, widest at top, top concave	12–25	F, S of *Cyanotis lanata*	Eichhorn et al. (2010)
Herbs — Commelinaceae	PRISMATIC upper part PSILATE, basal part SCROBICULATE	PRIS_PSI_SCROB	Prismatic shape with basal part scrobiculate and upper part psilate with concave facets, top flat or obliquely conical	12–30	F of *Commelina* spp.	Eichhorn et al. (2010)
Low diagnostic value	SPHEROID PSILATE	SPH_PSI	Spheroidal solid phytoliths with smooth surface.	5–25	L, W of certain dicotyledons, monocotyledons, gymnosperms and ferns	e.g., Neumann et al. (2019)

(*continued on next page*)

Table 2 (*continued*)

Plant group interpretation	Name (after ICPN 2.0[a])	CODE (after ICPN 2.0)	Description	Size (μm)	Anatomical origin[b]	References
	BLOCKY	BLO	Compact, heavily built, solid phytoliths with length/width <2 and width and thickness roughly equal	35–150	Mainly in L of Poaceae and Cyperaceae but also in other parts of monocots and dicots.	e.g., ICPT: Neumann et al. (2019)
	ACUTE BULBOSUS	ACU_BUL	Unarticulated, solid body with a generally narrower, acute part (apex) and another, wider part (base).	25–100	L, R of grasses, sedges and other taxa	E.g., ICPT: Neumann et al. (2019)
	TRACHEARY	TRA	Elongate, cylindric or irregular shape with annular, helical, or pitted ornamentation	Length 15–150; width 5–30	Tracheary elements of mainly nongrass plants	E.g., ICPT: Neumann et al. (2019)
	ELONGATE ENTIRE	ELO_ENT	Elongated phytoliths with smooth margins and various transverse section (triangular, circular, parallelepipedal or tabular); L:W ≥ 2	10–150	L of monocotyledons, certain conifers, ferns	E.g., ICPT: Neumann et al. (2019)
	ELONGATE SINUATE	ELO_SIN	Tabular phytoliths with regular or irregular sinuated margins and various transverse section (triangular, circular, parallelepipedal or tabular); L:W ≥ 2	10–150	L of monocotyledons, certain conifers, ferns	e.g., ICPT: Neumann et al. (2019)
	ELONGATE DENTATE	ELO_DET	Elongated phytoliths with dentate margins and thickness ranging from tabular to robustly thick; L:W ≥ 2	15–150	Mainly in L of Poaceae but also in others plant families	e.g., ICPT: Neumann et al. (2019)
	ELONGATE DENDRITIC	ELO_DEN	Elongated phytoliths with dendritic margins and various transverse sections (from tabular to circular); L:W ≥ 3	15–100	Mainly in I of Poaceae but also in L of grasses, other monocotyledons and certain dicotyledons	e.g., ICPT: Neumann et al. (2019)

[a] International Code for Phytolith Nomenclature 2.0 (ICPT: Neumann et al., 2019).
[b] F = fruits; S = seeds; L = leaves; I = inflorescences; R = roots; W = wood.

lowest D_0 values, as suggested by Thomsen et al. (2016). The final dose was chosen in the D_0-plateau area. The ratios of recovered to given dose are consistent with unity at two sigma for all samples but RB5 (Table 3). This sample was not tested any further; preliminary measurements suggested that it was very recent (less than 5000 years). The equivalent dose for the other samples then was measured on 1100 to 1200 grains.

The dose rate is the sum of the contribution from the cosmic, the gamma, and the beta dose rates. The alpha dose rate was assumed negligible since the samples had been HF etched so that most of the outer layer of the grains irradiated by the alpha particles has been eroded before the equivalent dose measurements. The cosmic dose rate was calculated from the current burial depth of each sample, based on the equation of Prescott and Hutton (1994). The gamma dose rate was measured with a field gamma spectrometer: the gamma probe was inserted 30 cm deep into the section at the location where each sample had been taken. The spectra were analyzed following the threshold technique (Mercier and Falguères, 2007). The beta dose rates were calculated from the internal radioactive content of each sample, applying the specific dose rate conversion factors of Guérin et al. (2011) and the attenuation factors of Guérin et al. (2012). The internal radioactive content was measured on dried, finely crushed, and sealed samples using high-resolution gamma spectrometry. The gamma and beta dose rates must be corrected for moisture and carbonate content (Nathan and Mauz, 2008). This is further discussed in section 4.

3. Results

The results obtained by the multiproxy approach favored in this study first report stratigraphic, geomorphological, and paleoenvironmental data, followed by chronological and archaeological results. In this way, the set of contextual results provides the detailed framework for the MSA archaeological occurrence discovered at the Ravin Blanc I site.

3.1. Stratigraphy and sedimentary facies

The excavation exposed a section approximately 2.70 m high by 6 m long, revealing a succession of seven sedimentary units (Fig. 3). The substrate was not reached due to the rising water table at the bottom of the section.

Ravin Blanc I stratigraphy: Unit 1 (SU1; 0–70 cm) corresponds to a grayish unit consisting of coarse sands with numerous black ferromanganese gravels and white carbonate concretions in silty matrix. This is underlain by boulders of carbonate rocks developed

Table 3
Results for the dose recovery tests applied to the Ravin Blanc I samples.[a,b].

Sample	Given dose (Gy)	Pass criteria	Nonsaturated	Pass D_0	D_0 (Gy)	DRR		OD (%)	
RB1	198	139/600	89	16	150	1.06	±0.04	8	±3
RB2	198	118/600	95	20	150	1.02	±0.04	11	±3
RB3	198	109/600	65	10	120	1.04	±0.04	8	±4
RB4	40	100/600	100	100	–	0.97	±0.02	15	±2
RB5	4.4	27/600	27	27	–	1.05	±0.02	6	±2

[a] 'Pass criteria' show the number of grains that pass the acceptance criteria over the number of measured grains. 'Nonsaturated' shows the number of grains that pass the criteria and were not saturated. 'Pass D_0' displays the number of grains finally selected in the D_0 plateau.
[b] DRR: dose recovery ratio, ratio of measured to given dose; OD: overdispersion.

immediately on top of the siliceous limestones that locally form the substrate and must represent a level of dismantling and alteration of the substrate. Numerous chemically weathered archaeological artifacts are embedded in the upper part of the unit (40–70 cm).

Unit 2 (SU2; 70–122 cm) corresponds to a whitish unit with pebbles and carbonate powdery boulders in a silty-clay-sandy matrix. This unit fills an alluvial channel that is visible in the cross section of the gully. It also contains the archaeological material, mainly in its lower part.

Unit 3 (SU3; 122–150 cm) corresponds to a very homogenous and indurated yellow-green sandy-clayey silt with carbonate concretions and pisolitic gravels toward the top. The lower limit with SU2 is very sharp indicating a phase of erosion before the deposit of SU3.

Unit 4 (SU4; 150–170 cm) corresponds to a complex unit comprising reworked underlying clay boulders and gravels with scattered pebble. This unit erodes the underlying sediments of SU3.

Unit 5 (SU5; 170–222 cm) corresponds to a yellow-green silty unit with carbonate concretions and sandy pockets of pink color.

Unit 6 (SU6; 222–250 cm) corresponds to a reddish-brown silty sand with pebbles and archaeological artifacts that incised the lower unit.

Unit 7 (SU7; 250–270 cm) is a grayish-brown silty sand corresponding to the present soil.

Sedimentary facies through thin sections: The micromorphological study allowed for specifying the sedimentary and pedological features of the stratigraphic units (Fig. 4).

RB1 thin section from SU1 confirms the transition between an alteration horizon of the underlying siliceous limestones and the first fluvial deposits in the ravine. It shows fragments of limestones and fluvial quartz sands (150–200 μm) with blunt sandstone gravels in a matrix of micritic and microsparite carbonate silts corresponding to substrate alterations. The horizontal carbonate concretions indicate the presence of stagnant water, at least seasonally. The pedological features are mainly porosity of biological origin, indicating moderate post-depositional pedogenesis. The high carbonate content shows that the level of alluvial groundwater has always been very high until today, preventing the leaching of carbonate, which is usually very active in Sudanese environments.

RB2 thin section from SU2 shows a basal mass consisting of a micritic carbonate mud with fluvial detrital sediments consisting of fine to medium sands (100–200 μm), pisolitic gravels (300 μm to 2–3 cm) and fine- and coarser-grained yellowish sandstone pebbles of gray color. The sand contains grains of quartz, polycrystalline quartz, and feldspar. The porosity is mainly mechanical and the voids are filled with microsparite (20–50 μm) indicating partial leaching of carbonates from the basal mass. This indicates a drying up of the sediment, at least seasonally.

RB3 thin section from SU3 shows a basal mass made up of decarbonated sandy-clayey silts corresponding to quartz grains (20–40 μm) but integrating numerous hyaline papules. The coarse fraction is composed of quartz sand grains (>100 μm), some of which are very rounded (300–800 μm) and clearly show aeolian shaping, pisolitic gravels and reworked carbonate nodules. The porosity is partly collapsed but shows well-developed hyaline clay illuviations along the voids.

RB4 thin section from SU5 shows a silty-clay basal mass close to the previous one with reworked carbonate nodules and pockets of fine to medium quartz sand (50–500 μm). The pedological features consist simply of a few discontinuous slits and channels that show very weak pedality indicating an essentially colluvial sediment.

RB5 thin section from SU6 shows sandy loamy sediment with a poorly developed basal mass (<20% of the sediment). The sand grains are quartz (200–500 μm) and also correspond to pisoliths. The pedality of the sediment is well developed, corresponding to a macroporosity drawing polyhedral aggregates and locally a microstructure of chitonic type. Most voids are devoid of pedological features and some secondary voids are covered with hyaline clay or fine micritic coatings. The whole indicates a poorly developed pedogenesis with a tendency to vertisolization.

3.2. Phytolith analyses

Results are presented in a diagram form of the relative abundance of diagnostic morphotypes on their own sum (Fig. 5). This diagram is complemented by the relative abundances of non-diagnostic shapes calculated on the total sum of all particles counted. Despite their low diagnostic value, their analysis can be useful to identify similarities or dissimilarities between samples and to point to some vegetation change.

The RB1 sample testifies of an open environment dominated by Poaceae and herb morphotypes reaching as a whole 86% of the diagnostic abundance. The D/P index is very low (0.17). GSSCP are well represented with 57% while BULLIFORM FLABELLATES reach 22%. The absence of the POLYHEDRAL to CYLINDRICAL FACETATE morphotype and the low percentage reached by SPHEROID ORNATE and NODULAR/GRANULATE morphotypes (10% as a whole) suggest a weak presence of arboreal vegetation. SPHEROID ECHINATE morphotype produced by palms are also badly represented in the assemblage (only 3%). The most conspicuous feature is the high proportion of BILOBATE and CROSSES GSSCPs (25% and 4%). These morphotypes are characteristic of the Panicoideae subfamily and suggest the growing of mesophytic to aquatic grasses. The record of Cyperaceae (1.5%) and *Commelina* sp. (0.5%) morphotypes are in accordance with the development of a tall grass savanna adapted to humid climate conditions or high available soil moisture.

The RB2 phytolith assemblage attests of a still open vegetation but a little bit closer as suggested by the higher D/P value (0.33). Indeed, morphotypes classified in the woody dicotyledons class record 20.6%, and the morphotypes related to the grass and herbal vegetation reach 77.2% of the diagnostic abundance. The POLYHEDRAL to CYLINDRICAL FACETATE morphotypes appear with 7%. The SPHEROID ORNATE phytoliths are more abundant with 12.3% while NODULAR and GRANULAR morphotypes decrease strongly (<1%). GSSCP are less dominant with 39.5% and still dominated by BILOBATE suggesting humid conditions. Indeed, SADDLE GSSCP produced mostly by Chloridoideae subfamily, more adapted to arid conditions, are badly represented with only 5.3%. BULLIFORM FLABELLATE halves reach for this sample only 9% of the sum of the diagnostic phytoliths. The most relevant record is the high percentage from grass and sedge papillae (12.8% and 15.8%), because these morphotypes do not represent well in modern soils, even though the vegetation is dominated by these plants (i.e., sedges; Albert et al., 2006). It testifies of a wet vegetation dominated by Cyperaceae and Panicoideae species with some sparse arboreal vegetation on an extra-local scale. The non-diagnostic morphotypes support this result. Indeed, we observe a good representation of the ELONGATE morphotypes (25% from the total phytoliths sum) in particular the SINUATE, DENTATE and DENDRITIC often rare in phytolith assemblages. Despite their low diagnostic value, these morphotypes are common in the Poaceae, especially in the long cells of epidermis of the inflorescence bracts of grass species for the ELONGATE DENTATE and DENDRITIC (Novello and Barboni, 2015). ELONGATE SINUATE have also been observed in the leaf epidermis of Poaceae but also of Cyperaceae (Metcalfe, 1971; Fernandez-Honaine et al., 2009) and can be linked with the high percentage of the Cyperaceae morphotype for this sample. Cyperaceae are typical of wet environments with permanent water. The high abundance of the POLYGONAL SCROBICULATE with cone produced by Cyperaceae family attests of an aquatic vegetation allowed by humid climate conditions and/or high water table.

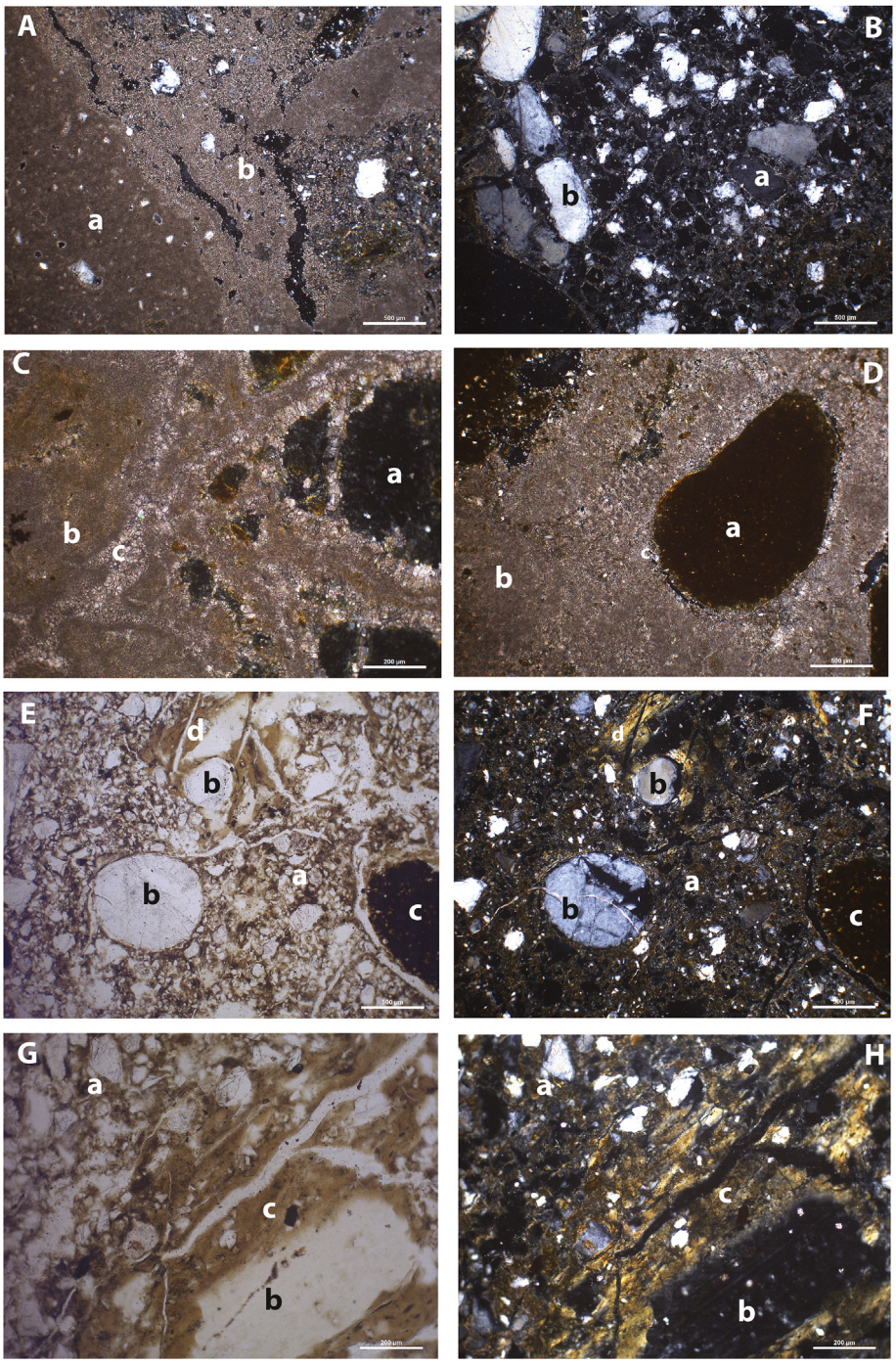

Figure 4. Microphotographs of thin sections from the Ravin Blanc I site. A. RB1, XPL, micritic groundmass (a) and late micritic secondary filling of large void (b); B. RB1, XPL, pocket of coarse alluvial sand (a, b); C. RB2, XPL, polycrystalline quarzitic sand (a) in a micritic (b), microsparitic groundmass (c); D. RB2, XPL, pisolitic gravels (a) in a micritic (b), microsparitic and sparitic groundmass (c); E. RB3, PPL, quartzitic silty sediment (a) with rounded aeolian sand grain (b), rare pisolitic gravels (c) and hyaline clay illuvial coating of voids (channels and chambers) with high birefringence; F. RB3, XPL, quartzitic silty sediment (a) with rounded aeolian sand grain (b), rare pisolitic gravels (c) and hyaline clay illuvial coating of voids (channels and chambers) with high birefringence; G. RB3, PPL, quartzitic silty sediment (a) with quartz coarse grain (b), pisolitic gravels (c) and hyaline clay illuvial coating of voids (channels); H. RB3, PPL, quartzitic silty sediment (a) with quartz coarse grain (b), pisolitic gravels (c) and hyaline clay illuvial coating of voids (channels). (For interpretation of the references to color in this figure legend, the reader is referred to the Web version of this article.)

The RB3 assemblage points to a change in the vegetation cover despite a D/P index similar to the previous sample (0.33). The morphotypes originating from the Poaceae and herbs are always dominant, representing 65% of the diagnostic phytoliths, while woody dicotyledon morphotypes make up to 22%. However, SPHEROID ECHINATE produced by Arecaceae (palms) increase with 12%. The composition of the GSSCP (40%) shows changes with the increase of the saddle GSSCP (12.5%) suggesting more arid conditions. BILOBATE are less abundant with 14.4%. BULLIFORM FLABELLATE record higher value with 23.2% while PAPILLAE, Commelinaceae and Cyperaceae phytoliths occur with low values (2% as a whole). For the non-diagnostic morphotypes, the most conspicuous feature is the high

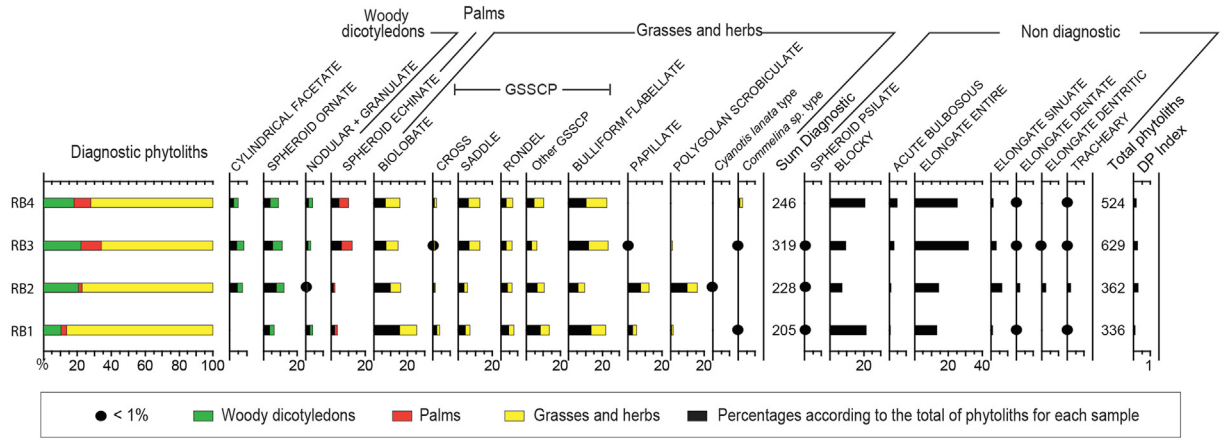

Figure 5. Phytoliths diagram of the Ravin Blanc I samples, RB1RB4. The percentages of diagnostic phytoliths in color bars in relation to the total diagnostic phytoliths. The bars in black represent the percentages of phytoliths in relation to the total phytoliths (diagnostic and non-diagnostic). For the phytolith morphotype classification used in the study, see Table 2. Detailed counts can be found in SOM Table S1. (For interpretation of the references to color in this figure legend, the reader is referred to the Web version of this article.)

percentage of the ELONGATE ENTIRE reaching 32% of the total phytoliths abundance. This could be explained by taphonomic processes. Indeed, Cabanes and colleagues (2011), who conducted an experiment on phytolith stability from modern and fossil samples, have shown that the poor preservation of phytoliths may be indicated by high proportions of ELONGATE ENTIRE. The breakage or/and dissolution of the phytoliths may cause the loss of the decoration of some long cell phytoliths and increase the representation of the more regular shapes. However, our phytolith assemblage is relatively rich and diversified. The fact that other long cells have been identified corroborates the good preservation of the phytoliths. This indicates that, if dissolution affected the phytolith assemblage, it was not extensive enough to bias the representativeness of the whole data set. To conclude, the phytolith assemblage of this sample indicates a change in the vegetation composition and cover with the transition to less humid conditions, at least during seasonal periods. Indeed, the strong decrease in Cyperaceae phytoliths testifies of the disappearance of wetlands, and the decrease of the water table. The development of open vegetation with a good representation of dicotyledons and palms can be interpreted as an open gallery forest growing along the watercourse.

Although we cannot exclude the fact that the sediments of SU5 are from heterogeneous provenience, the RB4 phytolith assemblage is quite similar to the previous one. The D/P index is slightly lower at 0.27, suggesting a more open environment. Indeed, the POLYHEDRAL to CYLINDRICAL FACETATE morphotype and the SPHEROID ORNATE record lower percentages (5% and 9%, respectively), but in contrast NODULAR and GRANULATE morphotypes increase distinctly by 4%. These results suggest a change in the tree cover composition. SPHEROID ECHINATE are always well represented in the assemblage at 10%. It suggests the presence of palms, but the relative abundance of SPHEROID ECHINATE cannot be easily interpreted since palms are high phytolith producers and highly resistant to postdepositional processes (Bamford et al., 2006; Albert et al., 2015). The Poaceae and herbs phytoliths are dominant reaching 71% of the diagnostic abundance. LOBATES (BILOBATE and CROSS) are strongly represented in the GSCCP class (15% and 3%, respectively) as are the SADDLES (13%), suggesting the presence of both mesophytic and xerophytic species. Cyperaceae morphotypes are absent from the assemblages indicating the nonperennial conditions of water availability. Nevertheless, the good representation of the *Commelina* sp. morphotype (2.5%) may suggest the growing of wild weeds on a seasonally flooded floodplain or on a grass savanna located on the interfluves.

3.3. Dating control

The equivalent dose distributions display overdispersions between 53 ± 8% and 74 ± 9% for samples RB1, RB2, and RB3 (Table 4; Fig. 6). These values are high and a part of the dispersion could be attributed to the heterogeneous content of the samples (e.g., presence of carbonates; see Fig. 4). However, these distributions clearly display grains whose equivalent dose is too small (close to 0) for being attributed only to a low beta dose rate environment. The micromorphological analyses suggest pedogenesis, including bioturbations in particular in the SU3. Therefore, the finite mixture model (FMM) was applied. Sigma_b (overdispersion attributed to each component) was varied from 0.2 to 0.6 and the best fit was determined from the Bayesian Information Criterion and maximum likelihood estimation (Roberts et al., 2000). The model suggests that, for each sample, two populations are mixed while sigma_b is 0.4–0.5, the most important population gathering about 90% of the grains (Table 4). The equivalent dose distribution for RB4 is highly

Table 4
Results of the equivalent dose (De) measurements applied to the Ravin Blanc I samples.[a-b].

Sample	Pass criteria	Nonsaturated	Pass D_0	D_0 (Gy)	De CAM (Gy)		OD (%)		De FMM (Gy)		Proportion		Sigma_b	k
RB1	243/1200	141	25	140	175.4	±19.5	53	8	194.1	±18.8	0.92	±0.06	0.4	2
RB2	217/1100	129	27	140	155.0	±22.2	72	10	167.2	±17.4	0.96	±0.04	0.5	2
RB3	206/1100	124	39	120	148.9	±18.2	74	9	182.6	±13.5	0.89	±0.05	0.4	2
RB4	100/1200	100	100	–	7.2	±1.5	164	15		–	–	–	–	–

[a] 'Pass criteria' show the number of grains that pass the acceptance criteria over the number of measured grains. 'Non-saturated' shows the number of grains that pass the criteria and were not saturated. 'Pass D_0' displays the number of grains finally selected in the D_0 plateau, over the D_0 threshold value indicated in the fifth column.
[b] CAM: Central Age Model; OD: overdispersion; FMM: finite mixture model; proportion: ratio of grains in the main component over the total number of grains in the distribution; sigma_b: overdispersion of each component; k: number of components.

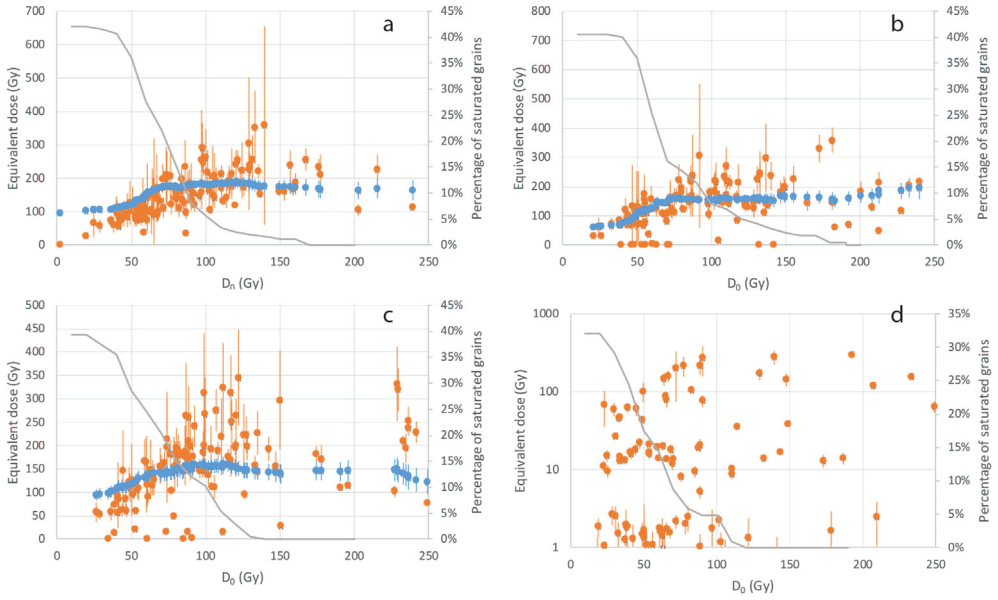

Figure 6. Equivalent dose distributions. a) RB1; b) RB2, c) RB3; and d) RB4. The orange points represent the equivalent dose as a function of the D_0 value for each grain that passes the selection criteria. Note that only the data for $D_0 < 250$ Gy are shown, but there are a few points beyond. The blue dots represent the Central Age Model (CAM) when the grains with the D_0 values lower than the one considered are discarded. The gray line shows the percentage of grains rejected because of saturation in function of the lowest D_0 value included in the population. The CAM calculation only serves here to show the impact of the low D_0 values. The finite mixture model was applied on grains beyond a threshold value, in the plateau region, where the proportion the grains rejected because of saturation is low (<5%). (For interpretation of the references to color in this figure legend, the reader is referred to the Web version of this article.)

dispersed (overdispersion: 176 ± 12%). The FMM suggests that three populations are mixed in similar proportion (which was already clear from simple visual inspection of the De distribution, Fig. 6). The mixing here is too important for calculating any significant age, since in that case the mean dose rate becomes meaningless. It can only be concluded that the three populations are, respectively, Pleistocene and early and late Holocene, based on the FMM equivalent doses and a dose rate between 1 and 2 Gy/ka. This admixture can be explained by colluvial nature of the sediments, and this sample is not discussed any further.

Here we comment only on the dose rates of samples RB1 to 3, although the data for RB4 and 5 are also displayed on Table 5. The K, U, and Th contents decrease slightly with depth. The sedimentological study suggests that the moisture history of the three samples is not similar: RB1 has been maintained in high water table, while RB2 and RB3 have been submitted to more variations (see sections 4.1 and 4.2). Meanwhile, the impact on the disequilibrium of the U chain seems moderate (Table 6). The activity of the pre-^{226}Ra part is in slight deficit compared with the post-^{226}Ra part for RB1 (pre-^{226}Ra to post-^{226}Ra activity ratio: 0.78 + 0.05) while the ratio of these activities is within 15% of unity for RB2 (0.87 ± 0.04) and RB3 (1.14 ± 0.07). While the origin of this moderate disequilibrium has not been determined, it can be estimated that this issue (that would induce a ca. ±6% variation on the dose rates depending on when the disequilibrium occurred) is by far outweighed by the water and carbonate content issue. A steady disequilibrium model is then used afterward.

Carbonates and water, which are present in the pores of the sediments, absorb a part of the radiations. Here we face several problems: these carbonates and water contents may have evolved during burial time and neither the timing of this change nor the initial and final water and carbonate contents are precisely known. The current carbonate content, while measurable, is not necessarily relevant for the beta dose rate calculation because of the heterogeneity of the carbonate distribution at the centimeter scale. Only the water content (mass of water over the mass of carbonated sediment) at the time of sampling was measured, but it is not necessarily close to the mean of the present water content (following seasonal and decennial variations). The micromorphological analyses, however, suggest scenarios on which we have built our estimates. RB1, RB2 were initially rich in carbonates, thanks to a high water table and the abundance of carbonates in the

Table 5
Dose rate data obtained for the Ravin Blanc I samples.[a–b].

Sample	Content							Dose rates (Gy/ka)					
	Water	K (%)		^{238}U (ppm)		^{232}Th (ppm)		Cosmic		Beta		Gamma	
RB1	12%	0.83	±0.01	1.46	±0.02	5.51	±0.05	0.146	±0.015	0.929	±0.081	0.562	±0.035
RB2	16%	0.94	±0.01	1.83	±0.02	6.22	±0.06	0.155	±0.016	1.034	±0.089	0.596	±0.038
RB3	22%	0.99	±0.02	1.87	±0.03	8.23	±0.10	0.168	±0.017	1.137	±0.095	0.615	±0.042
RB4	6%	0.74	±0.02	1.63	±0.03	6.93	±0.10	0.178	±0.018	0.969	±0.079	0.598	±0.038
RB5	3%	0.59	±0.02	2.80	±0.04	8.14	±0.09	0.190	±0.019	0.978	±0.070	0.625	±0.041

[a] Water: mass of water at the time of sampling over the mass of dry sediment, including carbonates. The K, U, and Th contents were measured on a portion of the dried and crushed sample with high-resolution gamma spectrometry.
[b] The beta dose rate is calculated from the K, U, and Th content (see main text), without any correction for water and carbonate contents and only serves as a base for further calculations. The gamma dose rate was measured with a field gamma spectrometer and takes into account the water and carbonate content at the time of measurement.

Table 6
K content and Th and U activities calculated from high-resolution gamma spectrometry measurements.

	Samples	RB1	RB2	RB3	RB4	RB5
Content	K (%)	0.83 ± 0.01	0.94 ± 0.01	0.99 ± 0.02	0.74 ± 0.02	0.59 ± 0.02
Activities (Bq/Kg)	^{232}Th	22.3 ± 0.2	25.1 ± 0.2	33.3 ± 0.4	28.0 ± 0.4	32.9 ± 0.4
	^{238}U head[a]	14.1 ± 0.8	19.7 ± 0.9	26.2 ± 1.6	27.0 ± 1.6	29.9 ± 1.5
	^{238}U middle[b]	18.0 ± 0.2	22.6 ± 0.2	23.1 ± 0.4	20.2 ± 0.4	34.6 ± 0.5
	^{238}U end[c]	16.6 ± 1.3	22.4 ± 1.6	20.8 ± 2.6	27.2 ± 2.8	27.1 ± 2.5

[a] Corresponds to the pre-^{226}Ra and is deduced mainly from the^{234}Th and^{235}U peaks.
[b] Corresponds to the post-^{226}Ra, calculated from the^{214}Pb and^{214}Bi peaks.
[c] Corresponds to the bottom of the chain, calculated from the^{210}Pb peak.

substratum. RB3 is a poor carbonated fluvio-aeolian sediment and furthermore, a nearly full decarbonation occurred in relation with pedogenesis and infiltration of meteoric water, while for RB1, the presence of the carbonates suggests a constant high water table, which allowed their preservation during burial. For RB2, an intermediate scenario is likely. Therefore, for RB1, we have assumed a constant dose rate, close to the current one. For RB2 and RB3 we have calculated two dose rates, one where the carbonate content was close to saturation, the other one where the carbonate content is lower, as today. Since these contents are not precisely known, large boundaries have been considered (see Table 7). The ages calculated for RB2 and RB3 correspond to either the case where the decarbonation occurred only recently or the case where the decarbonation occurred soon after deposit. The most likely age stands within these extreme cases.

The final estimates are given in Figure 7. For RB1, the age estimates range between 124 ± 12 ka and 128 ± 12 ka. For RB2 and RB3 the minimal estimates are 99 ± 12 ka and 102 ± 10 ka, respectively, while the higher estimates go up to 137 ± 17 and 148 ± 15 ka, respectively. Since the age of RB2 and RB3 are necessarily younger than RB1, it can be concluded that RB1 (SU1) was deposited at the beginning of stage 5, during MIS 5e (130–123 ka), while RB2 (SU2) and RB3 (SU3) were deposited sometime between the beginning of stage 5 and 92 ka, probably between MIS 5d (123–109 ka) and MI 5b (96–87 ka). The archaeological artifacts are, in any case, clearly dated to the beginning of the last interglacial period.

3.4. The Middle Stone Age lithic assemblage

Assemblage composition: For a total of 1136 artifacts (Table 8), flakes are by far the most common artifact type. By contrast, blades—which refer to flakes with length equal to or larger than twice the width—are infrequent as are the cores. The hammerstone gives complementary information on the production technique (Fig. 8C). The relatively high amount of angular debris relates to the knapping activities, but it may also partly represent knapped elements that were too weathered to be identified.

The artifacts are generally of medium size (Table 9), with a low representation of small pieces ≤3 cm. The unbroken small pieces make up to 24% of the complete flakes, which is relatively low for an assemblage in which knapping activities are identified. This underrepresentation of small elements is likely to be linked to the significant moisture rate and more generally, the water action identified for the sediments containing archaeological horizon. Water action may have washed away part of the smallest pieces or led to the disintegration of part of these, due to nearly permanent contact with water over the long term (see de la Torre et al., 2018). However, the high water table characterized in SU1 and the calm water environment representing a low-energy river flow in SU2 (see sections 4.1 and 4.2) have probably led to minor relocation of the larger artifacts.

All retouched tools are made on flakes (n = 40/44 tools) except one made on a blade. The shaping technical process (n = 3/44) is also recognized and represented by one biface and two bifacial pieces, i.e., a blank with bifacial shaping scars, irregular in shape.

Raw material and preservation: All lithics are made of sandstone, except one blade made of green chert (also called silexite), and three lithics are made of brown granite, the latter including the hammerstone. Sandstone is available in the direct vicinity of the site, in primary and secondary outcrops originating from banks occurring in the schist-pelitic sedimentary series that form the bedrock, as part of the various grauwacke formation (see section 2.2). The raw materials seem to encompass variable knappability as internal cracks are visible on fracture surfaces of part of the flakes. During the sampling of local raw material sources, it was noticed that the available sandstone, appearing in primary outcrops as much as in secondary position in the form of angular blocs or angular cobbles, is particularly hard to fracture. Fracturing the natural rock requires a high amount of force and an appropriate striking angle. In some cases, the sandstone from the modern sources also split in clear breaks, which could also explain the slab-like surfaces observed on some lithic artifacts worked at the Ravin Blanc I site.

The closest source of granite cobbles is probably the Falémé river bank, at less than 2 km from the site, although not in the currently visible thick (1–3 m) cobble deposit at the base of the sequence, which is much more recent than the Ravin Blanc I occupation (Davidoux et al., 2018; Rasse et al., 2020). Chert availability is difficult to locate precisely, although banks of this raw material are present within the local bedrock (see section 2.2). The closest yet identified primary outcrops are located in a range of 5–10 km from the site.

Although sandstone is the dominant raw material type used at the Ravin Blanc I site, it has different surface appearances. The cement of the sandstone contains more or less silica or limestone, which has strongly impacted the preservation of the lithic artifacts in the context of extreme hydrometric conditions characterizing SU1 and 2. The higher is the silica content in the sandstone cement, the greater is the preservation of the sharpness of the cutting edges and of the negative scars. The lithics made of sandstone with higher rates of limestone cement have blunted edges and a soapy appearance that makes it sometimes difficult to characterize the technical traces. Another sandstone used at the Ravin Blanc I site

Table 7
Initial and present water and carbonate contents (percentages).

Sample	Water or carbonate contents			
	$\frac{mc1}{ms}$	$\frac{mw1}{ms}$	$\frac{mc2}{ms}$	$\frac{mw2}{ms}$
RB1	50 ± 10	15 ± 5	50 ± 10	15 ± 5
RB2	25 ± 10	15 ± 5	50 ± 10	15 ± 5
RB3	5 ± 2	15 ± 5	40 ± 10	15 ± 5

m_s: mass of dry sediment; m_w: mass of water; m_c: mass of carbonates. See SOM S1 for calculation of the correction for water and carbonate contents.

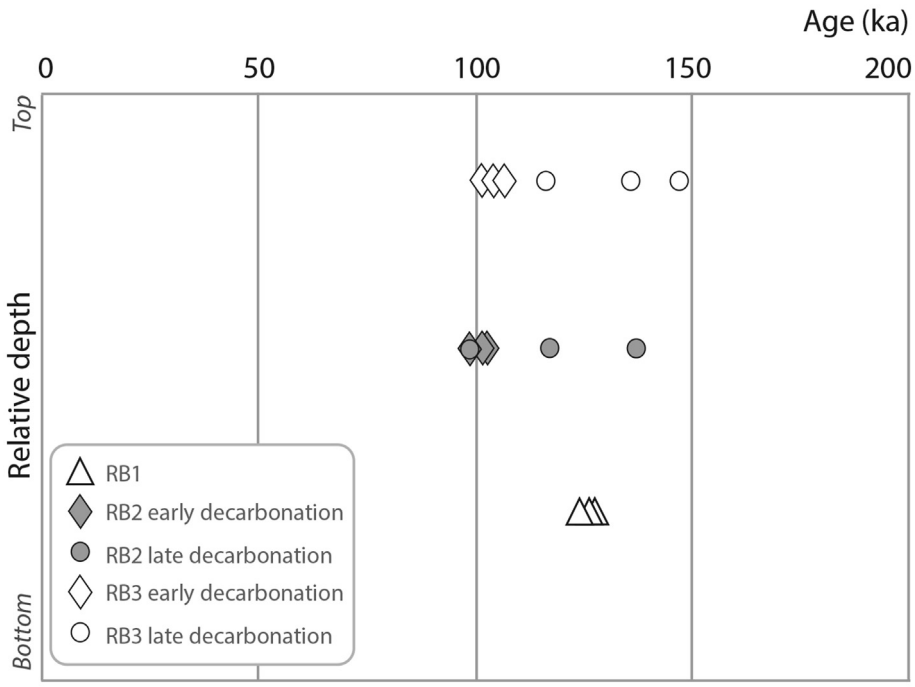

Sample		RB1	RB2		RB3	
			Early decarbonation	Late decarbonation	Early decarbonation	Late decarbonation
Age (ka)	A)	124 ± 15	99 ± 12	99 ± 12	102 ± 10	147 ± 15
	B)	126 ± 15	101 ± 13	117 ± 15	104 ± 11	136 ± 14
	C)	128 ± 15	102 ± 13	137 ± 17	107 ± 11	117 ± 12

Figure 7. Final age estimates for RB1, RB2, and RB3 samples from the Ravin Blanc I site. For RB1, only a model where the high water and carbonate content have been steady over time is considered. For RB2 and RB3 two extreme scenarios have been considered: either the decarbonation occurred early after deposition and low carbonate content (but variable water contents) have prevailed or the decarbonation occurred recently and saturated values of carbonate and water have prevailed. Several points are presented for each model, calculated from middle and boundaries for the carbonate and water contents in each case. In the table, (B) corresponds to the central values for water and carbonate content estimates while (A) and (D) correspond to the lower and the upper boundaries of the estimated water and carbonate contents, respectively.

has a coarse-grained appearance due to visible sand grains. Surface patina is invariably chalky white, pasty when wet, except for eight sandstone lithics that are disintegrating following significant fissuring, showing an ultimate stage of alteration.

For the aim of this study, we have subdivided sandstone types according to arbitrary qualitative observations on the micro-topography of the surfaces and their state of weathering. Fine-grained and middle-to fine-grained sandstone dominate the assemblage (Table 10).

Knapping technique and platform types: The knapping technique is handheld hard stone percussion, possibly with granite hammerstones such as the one represented in Figure 8C. Bulbs are very pronounced, and significant lancets (or fissures) are often visible along the blank ventral faces. The angle between the platform and the dorsal face is most often open, and provides values between 85 degrees and 90 degrees. The platforms are thick due to an impact point applied away from the core edge, probably to avoid the breakage of the edge, as the platforms are most often unprepared (60% plain platforms; total $n = 334$). Striking platform preparation is relatively rare as faceting was identified on only 5% of identifiable platforms. Dihedral platforms, which show a minimal striking platform preparation by large removals, are slightly more numerous (16%). Platforms that were shattered or partly broken at impact (12%) are also represented, probably as a result of an impact point that was too close to the core edge.

Table 8
General composition of the lithic assemblage at the Ravin Blanc I site.

	Sample size	%
Flakes	945	83.2
Blades	31	2.7
Cores	11	1
Hammerstone	1	0.1
Biface and bifacial pieces	3	0.3
Angular debris	145	12.8
Total	**1136**	**100**

Blank production methods: The assessment of blank production methods relies on more than a third of the total amount of flakes retaining informative technological characteristics, as well as on the blades and cores (Table 11). Several core reduction methods representing different volumetric conceptions were identified.

The first identified *chaîne opératoire* of production is grounded in a Levallois conception of flaking (see e.g., Boëda, 1995; Mourre, 2003). It consists of preparing cores with hierarchized surfaces, opposing a convex striking platform surface to a flatter exploitation surface from which blanks are removed parallel to the intersection

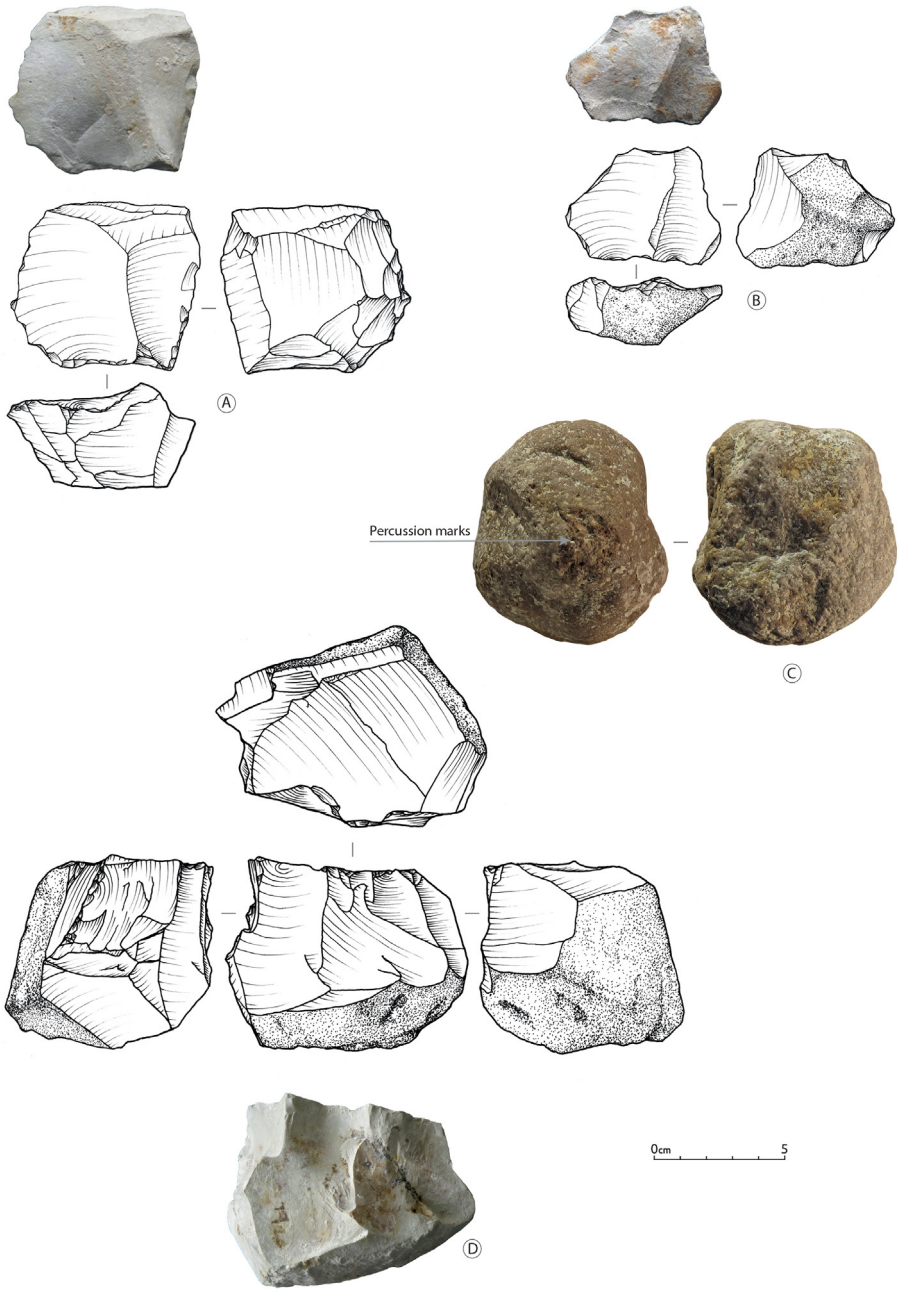

Figure 8. Examples of core types and hammer-stone found at the Ravin Blanc I site. A, B: Levallois unidirectional cores, sandstone. C: Hammerstone with localized pitting, granite. D: Orthogonal core, sandstone. Drawings: Heike Würschem. (For interpretation of the references to color in this figure legend, the reader is referred to the Web version of this article.)

line between the two surfaces. Two main recurrent Levallois methods are implemented. The unidirectional Levallois method (Fig. 8A, B) is used for producing unidirectional flakes that are slightly elongated. In view of the low number of scars on the dorsal face of blanks (average $n = 2.5$) and of the scars visible on the cores' exploitation surfaces, few removals seem to be produced per series. Lateral convexities are managed by débordant removals that possibly both favored a longer exploitation of each core, and

Table 9
Dimensions of unbroken artifacts at the Ravin Blanc I site.

	Sample size	Length (mm)				Width (mm)				Thickness (mm)			
		Max.	Min.	Mean	St. dev.	Max.	Min.	Mean	St. dev.	Max.	Min.	Mean	St. dev.
Flakes	188	105	15	47	18.6	115	15	45	18	29	4	12	7.2
Blades	16	115	38	66	22	70	18	33	12.8	27	10	13	5.4
Cores	5	130	55	83	NA	95	50	72	NA	85	36	41	NA
Tools	20	110	30	58	21.3	90	20	52	17.2	37	13	19	8

Max = maximum; min = minimum; st. dev. = standard deviation; NA = not applicable.

Table 10
Distribution of raw material types at the Ravin Blanc I site.

Raw material	Sample size	%
Sandstone, very fine-grained	119	*10.5*
Sandstone, fine-grained	419	*36.9*
Sandstone, middle to fine-grained	448	*39.4*
Sandstone, coarse-grained	138	*12.1*
Sandstone, disintegrating	8	*0.7*
Granite, brown	3	*0.3*
Chert, green	1	*0.1*
Total	**1136**	***100***

compensate for the small number of removals produced during each series. A similar pattern is observed for centripetal Levallois core reduction. Removals are invasive and leave few numbers of dorsal scars on flakes. The occurrence of débordant edges among the centripetal flakes (21% of the centripetal flakes) is close to the ratio of débordant edges occurring in the unidirectional method (24% of unidirectional flakes). Unidirectional convergent flakes are only represented by end-products, indicating that their production occurred at a specific stage of the core reduction sequence. Their characteristics may indicate that they are mostly produced by a Levallois production method, possibly during the unidirectional exploitation.

The second identified 'chaîne opératoire' of production consists of a volumetric exploitation of angular natural rock volumes. This method shows unidirectional extractions on a surface that is orthogonal to the striking platform following an algorithmic reduction. The algorithmic reduction entails that each exploitation surface created by one or several removals becomes a striking platform for a new series of unidirectional removals (see Forestier, 1993). The exploitation surfaces likely provided most of the blades of the assemblage, including the first blades, and could additionally provide for some unidirectional convergent flakes. One core shows a quite long series of removals on the exploitation surface, with lateral removals aiming at managing the lateral convexities (Fig. 8D), but the others are simpler and show only the extraction of two to three elongated blanks.

Apart from a few exceptions, most of the unidirectional blanks do not provide for clear-cut characteristics that would allow for attributing the flakes to one or the other chaîne opératoire. This is due to the fact that the hard hammer percussion set back from the core edge, the unprepared striking platforms, and the expected thickness of the unidirectional flakes, are close for both production methods, Levallois and volumetric.

Other methods are also represented such as the Kombewa method that demonstrates the exploitation of flakes as core blanks. The Kombewa method at Ravin Blanc I is likely circumstantial rather than highly predetermined as it is for the industries that provided for the definition of this method (Owen, 1938). One flake morphology resembles a discoid flake, but due to the absence of other discoid flakes or cores, it was likely produced by a non-discoid exploitation, probably Levallois centripetal.

Due to the high number of flakes with indeterminate technological characteristics, it is possible that additional knapping methods have been implemented at the Ravin Blanc I site resulting in undiagnostic products, although most pieces have suffered the aforementioned issues related to taphonomy.

Formal tools: The toolkit contains high proportions of blanks with notches, either localized or in series, and creating denticulated edges or borer beaks. Other retouched blanks include side- and end-scrapers as well as blanks with localized retouch. Three pieces bear invasive scars that relate to a process of partial shaping (façonnage) of large blanks.

Among the pieces with a single notch, four are particularly interesting as they show a single large retouched notch that created a concave edge on the blanks (Fig. 9A–C). These notches are made by short direct removals, that is, directed from the ventral face to the dorsal face, that are usually abrupt or abrupt to semi-abrupt in one case. These large notches do not seem to be applied to a specific blank type in terms of technology, but they are implemented on blanks with a thick midsection, creating a robust large notch.

Other notched pieces are more often made by Clactonian removals, equally direct or inverse when single, and equally direct and combined direct-inverse when multiple. Multiple notches are differentiated from denticulates by the fact that the notches are applied to the opposite cutting edges of the tool blank. In addition, notches of denticulated pieces are always of short extent, while those applied to other pieces can also be of medium extent.

Two notched pieces, among which the one with a combination of a Clactonian and a retouched notch (Table 12), show that the retouch was applied close to the tip of the triangular blanks, creating a half-beak (Fig. 10D). Two formal borers were recognized in the assemblage, made by opposed retouched notches (Fig. 9G).

Regarding the scrapers, two relevant characteristics are noticed. First, the presence of end-scrapers with a large front made by semi-abrupt direct retouch of medium extent and made on blanks of uniform thickness resembling regular slabs, or heavily retouched

Table 11
Detailed technological categories of the lithic artifacts of the Ravin Blanc I site. Percentages are given per category, and for flakes, blades, and cores they are calculated after the subtotals.

Technological category	Sample size	%
Flake, first flake ('entame')	7	0.7
Flake, unidirectional core management	12	1.3
Flake, centripetal core management	2	0.2
Flake, other core management	62	6.6
Flake, unidirectional end-product	95	10.1
Flake, centripetal end-product	67	7.1
Flake, unidirectional convergent end-product	18	1.9
Flake, Kombewa end-product	7	0.7
Flake, discoidal? End-product	1	0.1
Flake, unidirectional 'débordant'	23	2.4
Flake, centripetal 'débordant'	14	1.5
Flake, bidirectional 'débordant'	2	0.2
Flake, Kombewa 'débordant'	3	0.3
Flake, indeterminate 'débordant'	12	1.3
Flake, retouch fake	3	0.3
Flake, indeterminate	617	65.3
Subtotal, flakes	**945**	**100**
Blade, first blade on block angle ('entame')	5	16.1
Blade, first blade ('entame')	1	3.2
Blade, unidirectional core management	4	12.9
Blade, unidirectional end-product	17	54.8
Blade, centripetal end-product	2	6.5
Blade, unidirectional 'débordant'	1	3.2
Blade, indeterminate	1	3.2
Subtotal, blades	**31**	**100**
Core, unidirectional orthogonal	3	27.3
Core, Levallois unidirectional	2	18.2
Core, Kombewa	1	9.1
Core, opportunistic	3	27.3
Core, indeterminate fragment	3	27.3
Subtotal, cores	**11**	**100**
Chunks	**145**	**100**
Hammerstone	**1**	**100**
Biface and bifacial pieces	**3**	**100**
Grand total	**1136**	**100**

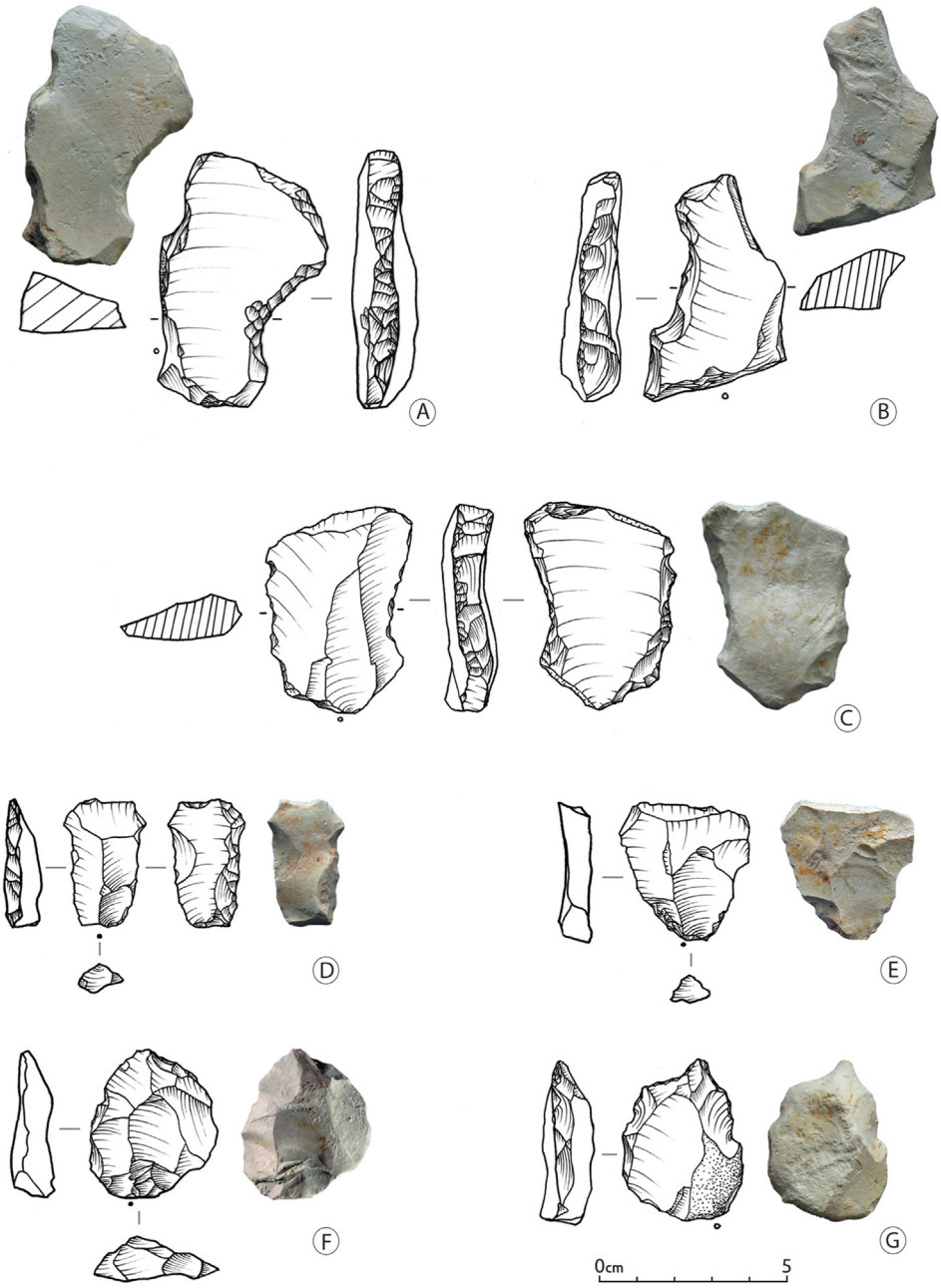

Figure 9. Examples of tools found at the Ravin Blanc I site. A, B: Thick blanks with single large retouched notch, direct semi-abrupt to abrupt retouch. C: Thick flake with single large retouched notch, inverse semi-abrupt to abrupt retouch. D: Side-scraper with inverse, semi-abrupt retouch. E: Flake with short direct retouch localized on proximal edges. F: Levallois centripetal flake. G: Beak on partly cortical flake. All in sandstone. Drawings: Heike Würschem. (For interpretation of the references to color in this figure legend, the reader is referred to the Web version of this article.)

flakes (Fig. 10C). Secondly, four of the seven side-scrapers show short inverse retouch, usually semi-abrupt, either combined with dorsal retouch or not (Fig. 9D). Among the blanks with localized continuous retouch, ventral semi-abrupt modification is also observed on 4 of the 9 tools, most often not combined with direct retouch. These inverse retouches, due to their short extension, do not aim at thinning the blank but rather modify the edge angle.

Finally, the assemblage contains three bifacially shaped pieces. The invasive removals show deep negative bulbs typical of hard hammer percussion. Shaping removals partially cover the dorsal and ventral faces of the blank, and two retain cortical areas on the dorsal surface. One is cordiform (Fig. 10A) but the two others are more irregular in shape and asymmetrical, which has led us to qualify them as bifacial pieces rather than as bifaces (Fig. 10B).

4. Discussion

4.1. Comprehensive view on the paleoenvironmental and chronological contexts of the Middle Stone Age occurrence

The combined approach led at the Ravin Blanc I, including large- and fine-scale geomorphological analyses, phytolith studies, geochronological and lithic analyses, shows that the site provides for unprecedented data on the beginning of the Upper Pleistocene in West Africa. Although this open-air site has a complex taphonomic and sedimentary history, which is a prevalent feature for the West African Paleolithic record (e.g., Allsworth-Jones, 2019), this study enabled an interpretation of the environmental dynamics at work over a maximum period of 140 to 92 ka, thus providing a

Table 12
Formal tool categories represented at the Ravin Blanc I site.

	Sample size
Notched blanks, single retouched	6
Notched blanks, single clactonian	4
Notched blanks, multiple clactonian	5
Notched blanks, combined single clactonian and single retouched	1
Denticulates	5
Borers	2
Side-scrapers	7
End-scrapers	2
Blanks with localized retouch	9
Bifacial pieces	2
Biface	1
Total	**44**

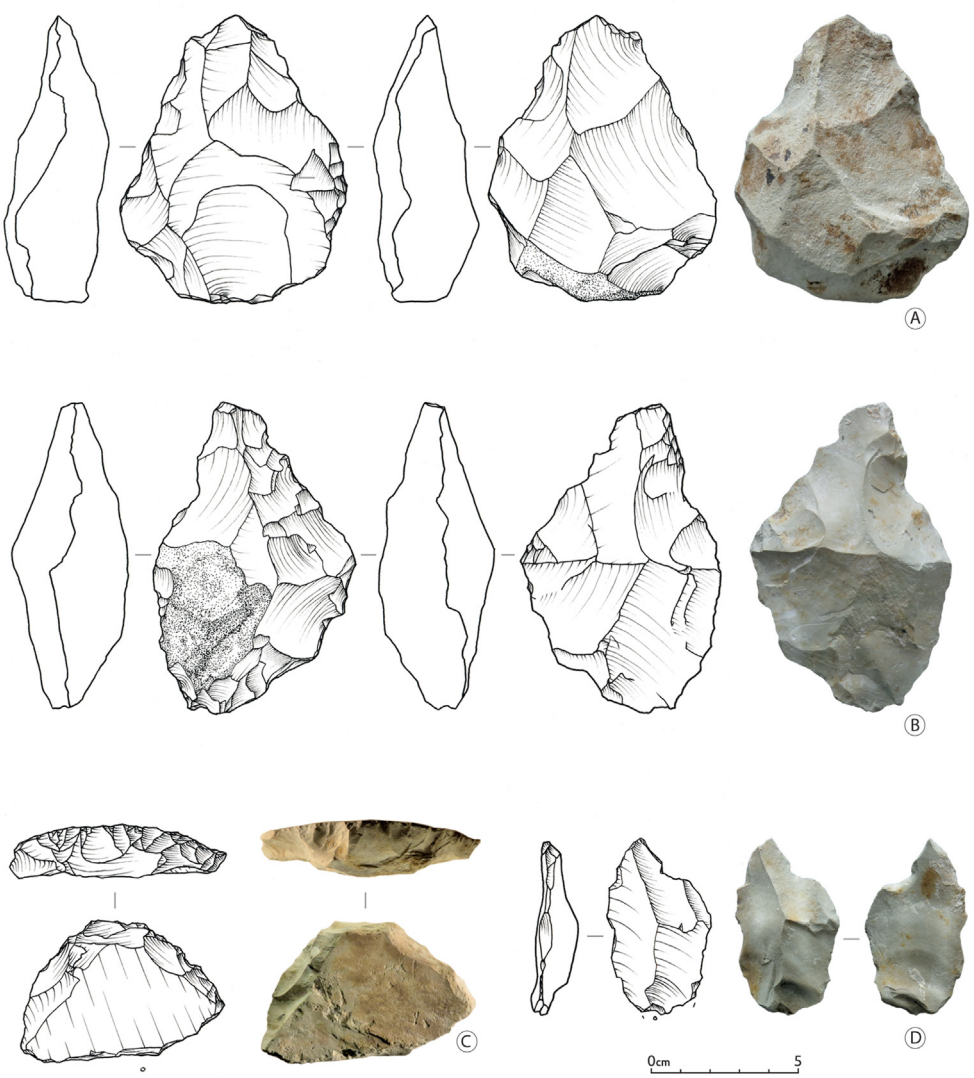

Figure 10. Bifacial tools, end-scraper and borer found at the Ravin Blanc I site. A: Biface. B: Irregular bifacial tools. C: Short and wide end-scarper. D: Borer on flake. All on sandstone. Drawings: Heike Würschem. (For interpretation of the references to color in this figure legend, the reader is referred to the Web version of this article.)

powerful contextual framework for the MSA archaeological occurrence of the Ravin Blanc I. Positioned in a channel system, the Ravin Blanc I archaeological site was affected by the water table oscillation and hydrological processes. Hydrological dynamics were important in the calculation of OSL date estimates, for which different moisture values and decarbonation scenarios have been taken into account. Two of the three samples (RB2 and RB3) therefore, provided early and late age ranges representing extreme scenarios based on the calculation of respectively late and early decarbonation and various water contents (Fig. 11). The data

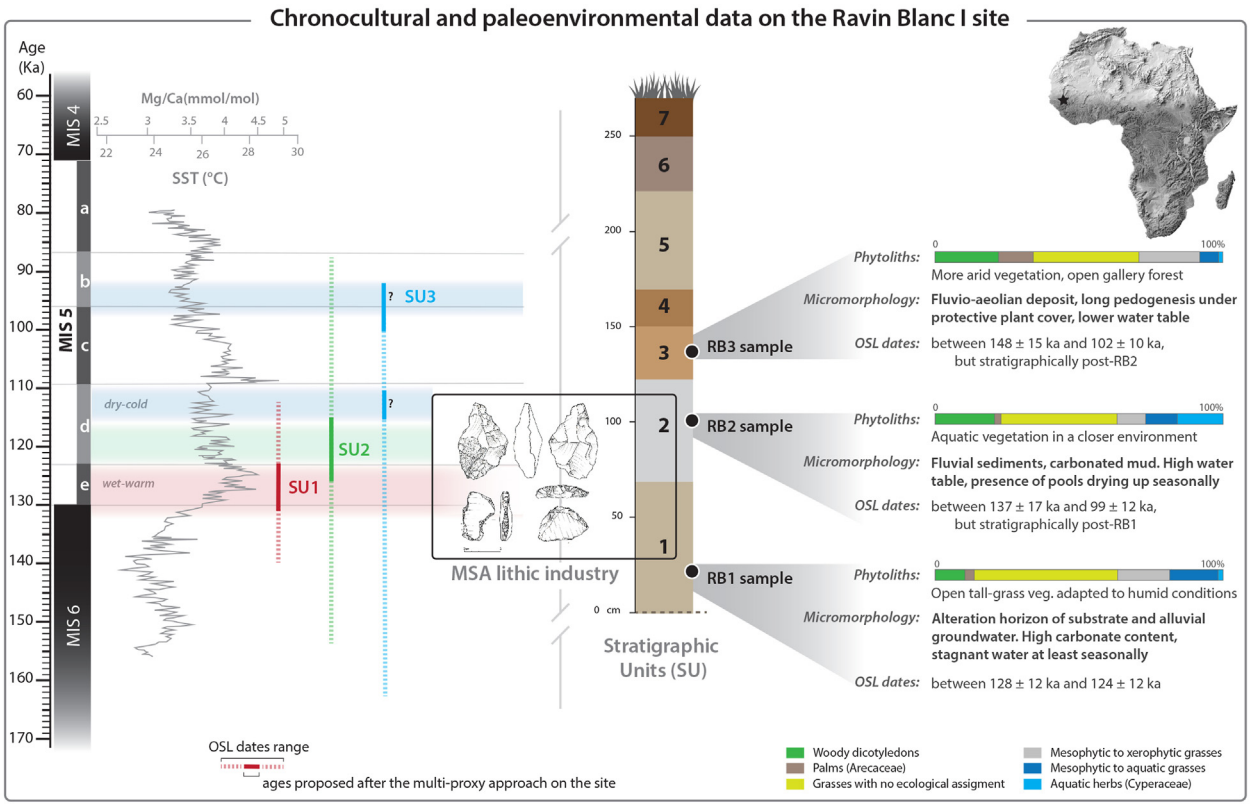

Figure 11. Schematic view of the chronocultural and paleoenvironmental data of the Ravin Blanc I site, eastern Senegal. The Mg/Ca (mmol/mol) and Mg/Ca-based SST estimates are from core MD03-2707, Gulf of Guinea, adapted from Weldeab et al. (2007). The early and late OSL date estimates for RB2 and RB3 represent extreme scenarios and reflect different decarbonation history. The most likely ages stand within these extreme cases, and their interpretation is presented in the form of solid color bars. The phytolith classification used here is after the method developed by Neumann et al. (2017). (For interpretation of the references to color in this figure legend, the reader is referred to the Web version of this article.)

obtained from the thin sections of the soil samples as well as the phytolith results for each stratigraphic unit, containing or not archaeological material, have allowed refining the age estimates by comparison with the paleoenvironmental data. From a taphonomic perspective, the lithic material shows weathered surfaces and the under-representation of small lithics. The smallest sized debris, which is usually abundant in knapping activities (e.g., de la Torre et al., 2018), was likely washed away by water activity or disaggregated due to immersion in water over a long duration as the groundwater at Ravin Blanc I has often been high. Nevertheless, despite these wet and carbonated conditions, the site revealed an exceptional preservation of the phytoliths, especially regarding the high proportion of sedge morphotypes which are usually not well preserved in soils (Albert et al., 2006; Novello et al., 2012). Moreover, Cabanes et al. (2011) suggest that the best indication of a well-preserved assemblage is the presence of abundant hairs, papillae and decorated long cells, which are rather well represented in the Ravin Blanc I samples. These results have led to the understanding of the timing and environmental context of the Ravin Blanc I human occupation.

First, the stratigraphic observations and micromorphological studies show that the fluvial channel of SU2 developed at the expense of the limestone substratum alterites and was filled by a carbonated mud fed with fluvial material, corresponding to the first recorded functioning of the Ravin Blanc. These results suggest that the archaeological material contained in SU1 would have been partially dismantled and re-deposited by SU2, probably over a short distance. Phytoliths in SU1 show that before this first functioning of the channel, the environment was rather open, with some arboreal vegetation, and characterized by a tall grass savanna adapted to moisture at a solid age estimate of between 124 ± 12 ka and 128 ± 12 ka, thus likely during MIS 5e (130–123 ka). The MSA occupation of the Ravin Blanc would therefore have taken place in a wet and locally semi-open environment, immediately adjacent to a permanent water source. Although fine-scaled data on paleoenvironments older than 60 ka are generally rare, this isotopic substage is identified as the first humid and warm period of MIS 5 in the region characteristic of the last interglacial period (Dupont et al., 2000; Weldeab et al., 2007).

Secondly, the carbonated mud of SU2 indicates the persistence of a high groundwater level with the presence of seasonal pools preventing complete carbonate leaching and suggests the regular functioning of a nearby carbonate source. Despite the presence of coarse alluvial deposits indicating medium-energy flooding, the high water level and the numerous diagnostic phytoliths of the Cyperaceae family indicate the expansion of a swampy environment. Riparian vegetation may also have been present on the edge of the wetland, in less saturated areas. These wet conditions identified in SU2 suggest that the early functioning of the channel was mainly characterized locally by a calm water environment with little more energetic river inflow. The date estimates for this fluvial phase offer a wide chronological window between 137 ± 17 ka and 99 ± 12 ka, which could thus take place between MIS 5e to 5c (ca. 109–96 ka). Due to its stratigraphic position above SU1 and the absence of a clear sedimentary hiatus between SU1 and SU2, it is likely that SU2 also relates to MIS 5e or to the beginnings of MIS 5d (ca. 123–109 ka). In any case, SU1 and SU2 concur in demonstrating that human occupation linked to SU1 took place during the

beginning of MIS 5, that is, at the beginning of the Upper Pleistocene.

Finally, the sediments of SU2 are covered by fluvio-aeolian deposits (SU3) that have partly eroded this lower unit. The stratigraphical observations and the micromorphological analyses highlight inputs of aeolian sediments and suggest a clear rupture in the sedimentary history. Sediments of SU3 have undergone a long pedogenesis of ferralitic-type leaching carbonates and testify to the lowering of the water table causing a decline in wetland. Based on similar sedimentological and micromorphological observations made for the Late Quaternary in the lower Falémé valley (Chevrier et al., 2020), this unit is interpreted as characteristic of a drier phase. RB3 phytolith assemblage also points to a change in vegetation cover, in particular to the development of open savanna dominated by Chloridoideae grasses. However, arboreal and palm phytoliths indicate the development of a more closed environment along the watercourse such as a galley forest, possibly by patches. Although the OSL dates largely overlap the ones obtained for previous SUs, with a range between 148 ± 15 ka and 102 ± 10 ka, the age estimates for RB3 show that the sediments from SU3 are in any case deposited at latest during MIS 5b (ca. 96–87 ka). As the observations clearly indicate a transition to a dry period and the data available regionally show a decrease of riverine runoff corresponding to the weakened West African monsoon system during MIS 5d or the start of MIS 5b periods (Dupont et al., 2000; Weldeab et al., 2007), we hypothesize that the environmental change toward drier conditions observed locally corresponds to one of those periods (Fig. 11). Although SU3 does not contain MSA material, the characterization of the paleoenvironmental conditions and its dating strengthen the interpretations of the lower units bearing the archaeological material.

The fact that the MSA archaeological occurrence at the Ravin Blanc I can be considered dating to an early humid stage of MIS 5 on solid grounds raises several questions. MIS 5 is seen as a period of behavioral changes in the evolution of *H. sapiens* in other parts of Africa where archaeological data are more abundant for this period, and the impact of the changing climatic conditions of MIS 5 on human behavior is a frequently addressed topic. At the scale of West Africa there is no other dated site relevant to MIS 5 and proposing a human evolution scenario based on the Ravin Blanc I site alone is currently not straightforward. However, some hypotheses are discussed below.

4.2. The importance of the MIS 5 for the evolution of the Middle Stone Age

There are two aspects to consider with respect to behavioral changes at work during MIS 5 in Africa. The first is that the considerable increase in moisture at the start of MIS 5 is accompanied by a wide variety of human responses and behavioral changes across Africa, and therefore an equally regional specific scenario may be expected for Senegal. In North Africa for example, in response to the new paleohydrological connections and newly formed biomes, more distinctive technologies have developed in relation with the broadening of inhabitable zones that have led to the occupation of more distant zones (Scerri, 2017). East Africa has shown a moderate increase in the variability of assemblage composition as an adaptative response to small-scaled expansions of hominin populations in a broader array of environments (Basell, 2008; Tryon and Faith, 2013; Blinkhorn and Grove, 2018). Conversely, the flexible and adaptative Lupemban composite technologies in Central Africa may have led to the persistence of the Lupemban through arid MIS 6 into the re-expansion of the lowland rainforests during MIS 5, although there is a lack of chronological control for the period covered by MIS 5 (Taylor, 2016). In contrast, South Africa shows highly contrasted techno-cultural patterns starting from MIS 5, including MSA I and 2 type industries as well as the development of the Still Bay and the Howiesons Poort (for synthesis see e.g., Wurz, 2013; Porraz et al., 2013).

Furthermore, on a larger scale, models of early *H. sapiens* dispersals at ca. 120 ka out of Africa as well as through Africa also emphasize the increasing movement dynamics at work during MIS 5 (see Groucutt et al., 2015 for synthesis; Rabett, 2018; Stewart et al., 2020). Our paleoenvironment results on the Ravin Blanc I site have shown that the Falémé Valley in Senegal, and probably more generally West Africa, has been affected similarly by the increased moisture rate observed on the continental scale (e.g., Blome et al., 2012; Kutzbach et al., 2020). Population adjustments to changed environments by increased mobility at the start of MIS 5 might have accounted for the characteristics of the industry as expressed at the Ravin Blanc I site. However, testing this hypothesis entails envisioning the Stone Age cultural sequence at work in West Africa on a broad chronological scale, which leads us to the second aspect to consider regarding the behavioral changes expected during MIS 5.

This second aspect is that the foundations of the behaviors observed in MIS 5 are to be sought in behavioral expressions that were displayed before this isotopic stage, i.e., at the end of the Middle Pleistocene. On one hand, the existence of a fully developed MSA is known as early as between ca. 400 ka and 300 ka elsewhere, such as at Jebel Irhoud in Morocco (Richter et al., 2017), ETH-72-8B at Gademotta in Ethiopia (Wendorf and Schild, 1974; Morgan and Renne, 2008), Katu Pan 1 in South Africa (Wilkins et al., 2012) or Olorgesailie in Kenya (Brooks et al., 2018). On the other hand, other examples show a late persistence of the Acheulean and the Sangoan almost all along the late Middle Pleistocene. At site 8-11-B at Sai Island in Sudan, there is an interstratification of Acheulean and Sangoan occupations between ca. 220 ka and ca. 150 ka (Van Peer et al., 2003), and in Ethiopia classic Acheulean industries have been securely dated to ca. 212 ka at Mieso (de la Torre et al., 2014), and ca. 160 ka at Herto (Clark et al., 2003; Sahle et al., 2019), while the MSA is fully developed in the same region. The cultural traits of the MSA therefore appear at very different ages according to the locations, although it seems that industries dating to MIS 5 in Africa are fully MSA, notwithstanding the great techno-typological diversity that this attribution includes. It appears, however, that the MIS 5 Ravin Blanc I industry retains technological traits inherited from older technical traditions, notably by the low representation of Levallois technologies and the presence of large and crudely shaped bifacial pieces. The hypothesis of a regionally specific evolutionary trajectory is therefore to be considered.

4.3. Is the MIS 5 marked by an early Middle Stone Age technology in West Africa?

In most of West Africa, the Stone Age sequence is very vaguely understood and as stated in Scerri et al. (2016:20), “the phases and their subdivisions are problematic.” Despite the critical lack of chronometric control, relative chronology confirms the presence of the Acheulean followed by different variants of MSA industries, in between which Sangoan type industries occur so far in sites located in southern West Africa, around the Gulf of Guinea, that is, Cameroun, Nigeria, Ivory Coast and Ghana (see Allsworth-Jones, 2019 for synthesis).

On one hand, the West African MSA has in the past also been designated as Mousterian or, at some places such as Adrar Bous in Niger, as Levalloisian Middle Paleolithic or early Middle Paleolithic (Clark et al., 2008). These names emphasize the strong Levallois and discoid component within the assemblages, resulting in industries dominated by products that are highly characteristic of the latter

methods, which is not the case at the Ravin Blanc I site. Elsewhere in Senegal, recent investigations along the Senegal River by Scerri and colleagues (Scerri et al., 2016, 2017) have led to the identification of several reliable yet undated MSA sites containing industries largely based on Levallois and discoid productions. Mousterian industries are considered preceding chronologically the Aterian in the northern latitudes of West Africa, maybe as early as from MIS 5 (Clark et al., 2008). While this chronological estimate for the Aterian based on analogies with North African chronologies matches the absolute dates obtained for the Ravin Blanc I site, the absence of pedunculated and bifacial foliate points in the assemblage, and the low standardization of the reduction methods, clearly indicate that they belong to incomparable technologies. The same statement applies to the comparison with more recent sites discovered in Senegal in the Falémé Valley and Tiemassas, as well as at Ounjougou and Yawa in Mali (see Table 1 for references).

On the other hand, industries bearing the much-disputed label 'Sangoan' (see Soper, 1965; Davies, 1976; Andah, 1979; Nygaard and Talbot, 1984; Lioubine and Guédé, 2000) are identified in southern West African sites but have not been found so far in Senegal, where they were not recognized as transitional facies between the Acheulean and the 'Mousteroid' MSA industries. The use of the term Sangoan in the West African context has been largely criticized, as in other African regions (e.g., McBrearty, 1988) besides Central Africa where it is the best described (Sheppard and Kleindienst, 1996; Barham, 2000; Clark et al., 2001). Its loose definition, the environmental determinism attributed to the Sangoan as being adapted to tropical forest environments, as well as the Sangoan main tool types (i.e., the core-axes or picks) considered 'ill-defined' (Andah 1979:63; Lioubine and Guédé, 2000), have led to alternative names such as 'Awudome Industry' (Davies, 1976), 'Sakumo Industry' (Andah, 1979), 'Asokrochona Industry' (Nygaard and Talbot, 1984) in West Africa. In terms of chronology, the site of Bete I at Anyama has provided a termimus post quem date for the Sangoan at 254 ± 51 ka (Lioubine and Guédé, 2000, Table 1), which is the oldest chronometric date available for the period usually assigned to the MSA in Africa. Notwithstanding the debates on nomenclature, important questions are raised regarding the presence of the large, crudely shaped bifacial pieces in the industry of the Ravin Blanc I site, which could easily fit in the category of core-axes, despite the loose definition of this typically Sangoan tool type. Another correspondence could be the presence of large concave side-scrapers, for which the presence of steep to blunt retouch is mentioned for the Sangoan Chipeta industry at Kalambo Falls, and could be akin to the widely notched pieces of the Ravin Blanc I (Davies, 1976; Clark et al., 2001). Furthermore, the Sangoan is also characterized by the absence or low numbers of Levallois-related artifacts compared with the mousteroid industries, which is another point of resemblance between the Sangoan and the Ravin Blanc I industry. Based on these observations, two scenarios can be suggested regarding the evolutionary dynamics that took place at the transition from the Middle to the Upper Pleistocene in Senegal.

The first scenario involves a late persistence of the Acheulean during most of the Middle Pleistocene followed by transitional industries as captured at the Ravin Blanc I site at the beginning of MIS 5, before the full development of the 'Mousteroid' MSA. In this case, the Ravin Blanc I assemblage would show a much-reduced emphasis on bifacial pieces in terms of technicity and abundance compared with the Acheulean, possibly compensated by the development of new tool types such as the pieces with large notches, and an increased importance of flake production through low-standardized reduction methods.

A second scenario would emphasize the aforementioned increased humid climatic conditions favorable to population movements as suggested for the start of MIS 5 to argue for a possible northward extension of Sangoan influences from the tropical margins of West Africa. In this case, the Ravin Blanc I assemblage would support a local interpretation of Sangoan technology by the introduction of crudely shaped bifacial pieces, before the development of fully classical 'Mousteroid' industries in the region. Since several other industrial traits of the Ravin Blanc I assemblage do not comply with its attribution to the Sangoan, namely the absence of spheroids and choppers (Davies, 1976; Allsworth-Jones 2019), there would only be external influences rather than a full development of the Sangoan in this area of West Africa.

In this regard, we would consider the assemblage of the Ravin Blanc I as representing an early stage of the MSA, following the same conception as for late Middle Pleistocene sites of East Africa located south of the Horn of Africa. There, the presence of heavy-duty tools (e.g., picks) is regarded as reminiscent of the Acheulean and as one of the main characteristics of the Sangoan, the latter marking the beginning of the MSA (see Tryon and Faith, 2013 for synthesis; McBrearty and Tryon, 2006). However, the dynamics that have led to the early MSA as seen at the Ravin Blanc I may have followed a different scenario than in East Africa, as presented above. Only new discoveries of archaeological sites dating from the Middle Pleistocene will allow a better assessment of which scenario is to be favored. For now, both scenarios are equally interesting in terms of regional evolutionary trajectories as they suggest that behavioral changes occurring through the Stone Age in West African may be in slight chronological offset compared with other regions of Africa.

4.4. An evolutionary trajectory with marked regional particularities

Data from several recently published studies appear to be consistent with the hypothesis of an offset in behavioral changes during the Stone Age sequence in West Africa compared with other regions in Africa (e.g., Scerri et al., 2016, 2017,2021; Niang et al., 2020), as well as with the presence of regional particularities in the developments of the MSA (e.g., Soriano, 2003; Soriano et al., 2010; Lebrun et al., 2016; Chevrier et al., 2016, 2018).

First, the Ravin Blanc I site contributes to the understanding of the West African chrono-cultural sequence by describing an assemblage that reproduces technical concepts better known for the Acheulean or the Sangoan, that is, crudely shaped bifacial pieces, into the Upper Pleistocene. Although the Ravin Blanc I site does not fully comply with the definition of the Sangoan sensu Davis (1976), the scenario of northward influences of the Sangoan could be corroborated by the site of Kokolo 2, located at Ounjougou in Mali, securely dated to the MIS 4 (Table 1). Kokolo 2 has provided an assemblage that was compared with several Oldowan assemblages (e.g., Nyabusosi and Olduwai sites DK and FLK North) to highlight their very strong resemblances (Soriano, 2003). It is characterized by quartz pebbles knapped by non-elaborated reduction schemes and by the importance of choppers and chopping tools. This description resembles the one of the Sakumo I industry—an alternative naming of the Sangoan—of the Asokrochona site in Ghana, for which strong parallels with several Oldowan industries have also been stressed by Andah (1979). These atypical industries, from which one at least has been dated to MIS 4, reinforces the vision of late occurrences of technological concepts better known for the Early Stone Age, at least that are not usually considered MSA (e.g., McBrearty and Brooks, 2000).

Second, important and complex behavioral dynamics have been stressed for the MIS 3 at Ounjougou and Yawa in Mali, which is to date the best-documented chrono-cultural sequence for this period

in West Africa (see Table 1; Soriano et al., 2010). Extremely varied technologies were discovered at different locations including bipolar-on-anvil, Levallois and algorithmic reduction strategies as well as blade productions, and which show the inconstancy of bifacial foliate point and heavy scraper productions. These highly diversified technologies as well as their rapid rhythm of change have led the authors to suggest that the Sahel experienced regular population movements during MIS 3, which contrasts with the ubiquity of the Aterian in North Africa and the Sahara for the same period (Soriano et al., 2010). It also contrasts with the cultural stability recently suggested for the coastal occupation of Tiémassas where the assemblages, based on Levallois and discoid productions, would have remained unchanged from 62 to 25 ka (Niang et al., 2020). These results raise the question of a possibly different behavioral evolution between inland and coastal areas of West Africa, and are a reminder that isolated sites are likely to yield an erroneous picture of the diversity of cultural expressions, or lack thereof, for a given period.

Third, a late persistence of the MSA until the Pleistocene to Holocene transition (MIS 1), first suggested based on the site of Ndiayène Pendao in the Senegal Valley (Scerri et al., 2016, 2017), has recently been confirmed by two newly discovered sites (Scerri et al., 2021). While the site of Ndiayène Pendao presented some dating problems due to the context of stratigraphic inversion that provided the two dates, ca. 11 ka apart, the site of Laminia, in the Gambia river valley, provides further evidence for a long-lasting MSA in the region (Table 1; Scerri et al., 2021). The site of Saxomununya, discovered in the upper Falémé valley, was dated to the Holocene (Table 1; Scerri et al., 2021), which shows a chronological overlap of the end of the MSA and the beginnings of the Late Stone Age (Lebrun et al., 2016).

Although the West African MSA therefore appears to show a regionally specific trajectory, this observation is still based on scarce and scattered data over time. Moreover, there is a complete gap of knowledge in Senegal as to the techno-cultural characteristics of Paleolithic occupations pre-dating MIS 5 following the Acheulean, the latter being itself only poorly described and undated. This justifies our choice to remain conservative and consider the Ravin Blanc I assemblage as displaying early MSA technological features in its largest sense. We also consider that new discoveries may point to the presence of markedly different technologies during the same period in other West African locations, as demonstrated for the MIS 3 at Ounjougou. Therefore, we cannot exclude the possibility that what has been considered in our study as reminiscent of the Acheulean, or influenced by the Sangoan, is in fact only the result of a phenomenon of convergence by reinvention. The Ravin Blanc I provides unprecedented data but the significance for the techno-cultural evolution of the West African Pleistocene populations remains to be clarified in the future.

5. Conclusions

The archaeological sequence relating to the West African MSA may not yet be sufficiently developed to allow large-scale comparisons such as those advocated by Will et al. (2019), but knowledge about this period has made a huge leap in the last ten years in the region. The West African MSA sequence has already shown an incomparable behavioral trajectory for a period from MIS 4/3 to 2, in the course of which a very wide variety of industries developed, undoubtedly reflecting complex population dynamics (Scerri et al., 2016, 2017; Chevrier et al., 2016, 2018; Niang et al., 2018). The MSA assemblage of the Ravin Blanc I, dated to MIS 5e, provides an unprecedented technology that may find groundings in Sangoan influences, or be a local post-Acheulean transitional industry, as crudely shaped bifacial pieces occur and Levallois technology is discrete. As the data is yet too scarce for understanding the relationship between the late Middle Pleistocene post-Acheulean industries and the assemblage of the Ravin Blanc I, we take a conservative stance and consider it as being of early MSA tradition. Indeed, the lithic industries available for Upper Pleistocene MSA in West Africa, but also in other regions in Africa, seem to be even more distinctive from the technology recognized at the Ravin Blanc I. Whether the environmental conditions have played a role in the development of the singular technology at the Ravin Blanc I site has not yet been determined, since comparative data on a regional scale is lacking. If we also consider the remarkable diversity of industries occurring during MIS 4/3 (e.g., Chevrier et al., 2016; Scerri et al., 2016; Niang et al., 2018) and the late persistence of the MSA in Senegal until the Pleistocene–Holocene transition (Scerri et al., 2017, 2021), then the model of a regionally specific expression of the late Middle and Upper Pleistocene human evolution could very well be confirmed. This model would be marked by local developments within the region as well as by the slight chronological offset of cultural and possibly biological changes compared with the trajectories of changes observed in other African regions. Current fieldwork carried out in the Falémé Valley in the framework of the Human Population and Paleoenvironment in Africa project on the late Middle Pleistocene sequence will likely allow for a more precise partioning of those dynamics in the future, by documenting the characteristics of the industries predating the Ravin Blanc 1 site on a local scale.

Acknowledgments

We would like to thank, for their financial support to Falémé Project, the Swiss National Science Foundation (application #101211-163022), the Franco-Swiss Lead Agency CHeRChA project (SNSF application # 100019E-164071; ANR 15-CE33-0009-01) as well as the Swiss-Liechtenstein Foundation for Swiss Archaeological Research Abroad (SLSA), and the Faculty of Sciences of the University of Geneva for the AFRI budget line. The Bordeaux Montaigne Doctoral School is also credited. We thank the Institut Fondamental d'Afrique Noire (IFAN) of the University Cheikh Anta Diop de Dakar (UCAD) and the UCAD students who participated in the fieldwork. We thank the excavation technicians from Dimmbal (Mali), whose work and commitment are indispensable to the success of this research, as well as the workers from the village of Toumboura who took part in the excavations at the Ravin Blanc site. We would like to thank the administrative and technical staff of the Laboratoire Archéologie et Peuplement de l'Afrique of the Anthropology Unit of the Department of Genetics and Evolution of the University of Geneva. Finally, we thank the Swiss Embassy in Senegal and the Swiss Cooperation Office in Bamako for their logistical support. We also thank the three anonymous reviewers and the editors of JHE who greatly contributed to the improvement of the manuscript, as well as Sylvain Soriano for his help on the data from the Malian Paleolithic.

Supplementary Online Material

Supplementary online material to this article can be found online at https://doi.org/10.1016/j.jhevol.2021.102952.

References

Andah, B.W., 1979. The Early Palaeolithic in West Africa: the case of Asokrochona coastal region of Accra, Ghana in perspectives on West Africa's past. West Afr. J. Archaeol. 9, 47–85.
Aitken, M.J., 1985. Thermoluminescence Dating. Oxford University Press, Oxford.

Albert, R.M., Bamford, M.K., Cabanes, D., 2006. Taphonomy of phytoliths and macroplants in different soils from Olduvai Gorge (Tanzania) and the application to Plio-Pleistocene palaeoanthropological samples. Quat. Int. 148, 78–94.
Albert, R.M., Bamford, M.K., Esteban, I., 2015. Reconstruction of ancient palm vegetation landscapes using a phytolith approach. Quat. Int. 369, 51–66.
Alexandre, A., Meunier, J.D., Lezine, A.M., Vincens, A., Schwartz, D., 1997. Phytoliths: indicators of grassland dynamics during the late Holocene in intertropical Africa. Palaeogeogr. Palaeoclimatol. Palaeoecol. 136, 213–229.
Allsworth-Jones, P., 2019. The Middle Stone Age of Nigeria in its West African context. Archaeopress, Oxford.
Bamford, M.K., Albert, R.M., Cabanes, D., 2006. Plio–Pleistocene macroplant fossil remains and phytoliths from Lowermost Bed II in the eastern palaeolake margin of Olduvai Gorge, Tanzania. Quat. Int. 148, 95–112.
Barboni, D., Bremond, L., Bonnefille, R., 2007. Comparative study of modern phytolith assemblages from inter-tropical Africa. Palaeogeogr. Palaeoclimatol. Palaeoecol. 246 (2–4), 454–470.
Barham, L., 2000. The Middle Stone Age of Zambia, South Central Africa. CHERUB, the Centre for Human Evolutionary Research, University of Bristol.
Basell, L.S., 2008. Middle Stone Age (MSA) site distributions in eastern Africa and their relationship to Quaternary environmental change, refugia and the evolution of *Homo sapiens*. Quat. Sci. Rev. 27 (27–28), 2484–2498.
Blinkhorn, J., Grove, M., 2018. The structure of the Middle Stone Age of eastern Africa. Quat. Sci. Rev. 195, 1–20.
Blome, M.W., Cohen, A.S., Tryon, C.A., Brooks, A.S., Russell, J., 2012. The environmental context for the origins of modern human diversity: a synthesis of regional variability in African climate 150,000–30,000 years ago. J. Hum. Evol. 62, 563–592.
Boëda, E., 1995. Levallois: a volumetric construction, methods, a technique. In: Dibble, H.L., Bar-Yosef, O. (Eds.), The Definition and Interpretation of Levallois Technology. Prehistory Press, Madison, pp. 41–65.
Bourel, B., Novello, A., 2020. Bilobate phytolith size matters for taxonomical and ecological identification of Chad grasses: a case study on 15 species. Rev. Palaeobot. Palynol. 275, 104–114.
Bøtter-Jensen, L., Andersen, C.E., Duller, G.A., Murray, A.S., 2003. Developments in radiation, stimulation and observation facilities in luminescence measurements. Radiat. Meas. 37 (4–5), 535–541.
Brooks, A.S., Yellen, J.E., Potts, R., Behrensmeyer, A.K., Deino, A.L., Leslie, D.E., Ambrose, S.H., Ferguson, J.R., d'Errico, F., Zipkin, A.M., Whittaker, S., Post, J., Veatch, E.G., Foecke, K., Clark, J.B., 2018. Long-distance stone transport and pigment use in the earliest Middle Stone Age. Science 360, 90–94.
Bullock, P., Fedoroff, N., Jonguerius, A., Stoops, G., Tursina, T., Babel, U., 1985. Handbook for Soil Thin Section Description. Waine Research Publications, Wolverhampton.
Cabanes, D., Weiner, S., Shahack-Gross, R., 2011. Stability of phytoliths in the archaeological record: a dissolution study of modern and fossil phytoliths. J. Archaeol. Sci. 38, 2480–2490.
Camara, A., Duboscq, B., 1983. Découverte et fouille d'un site acheuléen en stratigraphie à Sansandé (région de Tambacounda, Sénégal). Notes Afr. 180, 61–71.
Camara, A., Duboscq, B., 1984. Le gisement préhistorique de Sansandé, basse vallée de la Falémé, Sénégal. Approche typologique et stratigraphique. L'Anthropologie 88, 377–402.
Camara, A., Duboscq, B., 1987. Contexte chronostratigraphique des outillages du Paléolithique évolué dans l'Est du Sénégal. L'Anthropologie 91, 511–520.
Camara, A., Duboscq, B., 1990. La fouille d'un site acheuléen à Djita (basse vallée de la Falémé, Sénégal). L'Anthropologie 94, 293–304.
Casey, J., Sawatzky, R., Godfrey-Smith, D.I., Quickert, N., D'Andrea, A.C., Wollstonecroft, M., Hawkins, A., 1997. Report of investigations at the Birimi site in Northern Ghana. Nyame Akuma 48, 32–38.
Chevrier, B., Rasse, M., Lespez, L., Tribolo, C., Hajdas, I., Fígols, M.G., Lebrun, B., Leplongeon, A., Camara, A., Huysecom, É., 2016. West African Palaeolithic history: new archaeological and chronostratigraphic data from the Falémé valley, eastern Senegal. Quat. Int. 408, 33–52.
Chevrier, B., Huysecom, É., Soriano, S., Rasse, M., Lespez, L., Lebrun, B., Tribolo, C., 2018. Between continuity and discontinuity: an overview of the West African Paleolithic over the last 200,000 years. Quat. Int. 466, 3–22.
Chevrier, B., Lespez, L., Lebrun, B., Garnier, A., Tribolo, C., Rasse, M., Guérin, G., Mercier, N., Camara, A., Ndiaye, M., Huysecom, E., 2020. New data on early holocene settlement and environment in Sudano-Sahelian West Africa: interdisciplinary investigation at Fatandi V, Eastern Senegal. PloS One 15, e0243129.
Clark, J.D., Cormack, J., Chin, S., 2001. Kalambo Falls Prehistoric Site: The Earlier Cultures: Middle and Earlier Stone Age, vol. 3. Cambridge University Press, Cambridge.
Clark, J.D., Beyene, Y., WoldeGabriel, G., Hart, W.K., Renne, P.R., Gilbert, H., Defleur, A., Suwa, G., Katoh, S., Ludwig, K.R., Boisserie, J.R., Asfaw, B., White, T.D., 2003. Stratigraphic, chronological and behavioural contexts of Pleistocene *Homo sapiens* from Middle Awash, Ethiopia. Nature 423, 747–752.
Clark, J.D., Gifford-Gonzalez, D., Batkin, J., 2008. Adrar Bous: archaeology of a central Saharan granitic ring complex in Niger. Studies in Human Sciences 170. Royal Museum of Central Africa, Tervuren.
Collura, L.V., Neumann, K., 2017. Wood and bark phytoliths of West African woody plants. Quat. Int. 434, 142–159.
Corbeil, R., Mauny, R., Charbonnier, J., 1948. Préhistoire et Protohistoire de la presqu'île de Cap-vert. Bulletin de l'IFAN, série B, tome X 378–460.
Davidoux, S., Lespez, L., Garnier, A., Rasse, M., Lebrun, B., Hajdas, I., Tribolo, C., Huysecom, E., 2018. Les fluctuations environnementales des deux derniers millénaires en Afrique de l'Ouest: premiers résultats de l'étude des terrasses alluviales du ravin de Sansandé (vallée de la Falémé, Sénégal oriental). Geomorphology 24, 237–255.
Davies, O., 1976. The 'Sangoan' industries. Ann. Natal. Mus. 22, 885–911.
de la Torre, I., Mora, R., Arroyo, A., Benito-Calvo, A., 2014. Acheulean technological behaviour in the middle Pleistocene landscape of Mieso (East-Central Ethiopia). J. Hum. Evol. 76, 1–25.
de la Torre, I., Benito-Calvo, A., Proffitt, T., 2018. The impact of hydraulic processes in Olduvai Beds I and II, Tanzania, through a particle dimension analysis of stone tool assemblages. Geoarchaeology 33, 218–236.
Delibrias, G., Guillier, M.T., Labeyrie, J., 1974. Gif natural radiocarbon measurements VIII. Radiocarbon 16, 15–94.
Descamps, C., 1979. Contribution à la préhistoire de l'Ouest sénégalais. In: Travaux et Documents, vol. II. Université de Dakar, Faculté des Lettres et Sciences Humaines, Département d'Histoire.
Duller, G.A.T., 2003. Distinguishing quartz and feldspar in single grain luminescence measurements. Radiat. Meas. 37, 161–165.
Duller, G.A.T., 2015. The Analyst software package for luminescence data: overview and recent improvements. Ancient TL 33, 35–42.
Dupont, L.M., Jahns, S., Marret, F., Ning, S., 2000. Vegetation change in equatorial West Africa: time-slices for the last 150 ka. Palaeogeogr. Palaeoclimatol. Palaeoecol. 155 (1–2), 95–122.
Eichhorn, B., Neumann, K., Garnier, A., 2010. Seed phytoliths in West African Commelinaceae and their potential for palaeoecological studies. Palaeogeogr. Palaeoclimatol. Palaeoecol. 298 (3–4), 300–310.
Esau, K., 1965. Plant Anatomy, 2nd ed. Wiley, New York.
Fahmy, A., 2008. Diversity of lobate phytoliths in grass leaves from the Sahel region, West Tropical Africa: Tribe Paniceae. Plant Systemat. Evol. 270, 1–23.
Fernandez Honaine, M., Osterrieth, M.L., Zucol, A.F., 2009. Plant communities and soil phytolith assemblages relationship in native grasslands from southeastern Buenos Aires province, Argentina. Catena 76, 89–96.
Forestier, H., 1993. Le Clactonien: mise en application d'une nouvelle méthode de débitage s'inscrivant dans la variabilité des systèmes de production lithique du Paléolithique ancien. Paléo 5, 53–82.
Galbraith, R.F., Roberts, R.G., Laslett, G.M., Yoshida, H., Olley, J.M., 1999. Optical dating of single and multiple grains of quartz from Jinmium rock shelter, northern Australia: part I, experimental design and statistical models. Archaeometry 41, 339–364.
Garnier, A., Neumann, K., Eichhorn, B., Lespez, L., 2013. Phytolith taphonomy in the middle-to late-Holocene fluvial sediments of Ounjougou (Mali, West Africa). Holocene 23, 416–431.
Garnier, A., Eichhorn, B., Robion-Brunner, C., 2018. Impact de l'activité métallurgique au cours du dernier millénaire sur un système fluvial soudano-guinéen. Étude multi-proxy des archives sédimentaires de la vallée du Tatré (pays bassar, Togo). Géomorphologie 24, 257–276.
Groucutt, H.S., Petraglia, M.D., Bailey, G., Scerri, E.M., Parton, A., Clark-Balzan, L., Jennings, R.P., Lewis, L., Blinkhorn, J., Drake, N.A., Breeze, P.S., Inglis, R.H., Devès, M.H., Meredith-Williams, M., Bolvin, N., Thomas, M.G., Scally, A., 2015. Rethinking the dispersal of *Homo sapiens* out of Africa. Evol. Anthropol. 24, 149–164.
Guérin, G., Mercier, N., Adamiec, G., 2011. Dose-rate conversion factors: update. Ancient TL 29, 5–8.
Guérin, G., Mercier, N., Nathan, R., Adamiec, G., Lefrais, Y., 2012. On the use of the infinite matrix assumption and associated concepts: a critical review. Radiat. Meas. 47, 778–785.
Guilloré, P., 1980. Méthode de Fabrication Mécanique et en Série des Lames Minces. Institut National Agronomique, Département des Sols, Paris.
Hawkins, A., Casey, J., Godfrey-Smith, D., d'Andrea, A.C., 1996. A Middle Stone Age component at the Birimi Site, Northern Region, Ghana. Nyame Akuma 46, 34–36.
Huysecom, E., Mayor, A., Lorenzo Martinez, M., Nsangou De Limbepe, J.A., Bocoum, H., Camara, A., Chevrier, B., Garnier, A., Guindo, N., Hajdas, I., Kassogué, G., Kiénon Kaboré, T.H., Lebrun, B., Lespez, L., Loukou, S., Mercier, N., Pelmoine, T., Pollarolo, L., Rasse, M., Sankaré, F., Tribolo, C., Truffa Giachet, M., Vieugué, J., 2017. Milieux et techniques dans la Falémé (Sénégal oriental) et sondages au royaume d'Issiny (Côte d'Ivoire): Résultats de la 19ème année du programme «Peuplement humain et paléoenvironnement en Afrique», SLSA. In: Jahresbericht SLSA 2015. Fondation Suisse-Liechtenstein pour les Recherches Archéologiques à l'Étranger, Zürich et Vaduz, pp. 109–208.
Inizan, M.L., Reduron-Ballinger, M., Roche, H., Tixier, J., 1999. Technology and Terminology of Knapped Stone. Translated by J. Féblot-Augustins. CREP, Tome 5, Nanterre. International Committee for Phytolith Taxonomy (ICPT).
Neumann, K., Strömberg, C.A.E., Ball, T., Albert, R.M., Vrydaghs, L., Scott-Cummings, L., 2019. International code for phytolith nomenclature (ICPN) 2.0. Ann. Bot. 124, 189–199.
Kottek, M., Grieser, J., Beck, C., Rudolf, B., Rubel, F., 2006. World map of the Köppen-Geiger climate classification updated. Meteorol. Z. 15, 259–263.
Kutzbach, J.E., Guan, J., He, F., Cohen, A.S., Orland, I.J., Chen, G., 2020. African climate response to orbital and glacial forcing in 140,000-y simulation with implications for early modern human environments. Proc. Natl. Acad. Sci. U.S.A. 117, 2255–2264.
Le Bourgeois, T., Merlier, H., 1995. Adventrop: Les Adventices d'Afrique Soudano-Sahélienne. Éditions Quae, Versailles.
Lebrun, B., 2018. Définition du cadre chronologique des gisements préhistoriques de la vallée de la Falémé (Sénégal) et apport des nouvelles techniques de micro-

dosimétrie à la datation par luminescence. Ph.D. Dissertation,. University of Bordeaux 3.
Lebrun, B., Tribolo, C., Chevrier, B., Rasse, M., Lespez, L., Leplongeon, A., Hajdas, I., Camara, A., Mercier, N., Huysecom, É., 2016. Establishing a West African chrono-cultural framework: First luminescence dating of sedimentary formations from the Falémé Valley, Eastern Senegal. J. Archaeol. Sci. Rep. 7, 379–388.
Lebrun, B., Tribolo, C., Chevrier, B., Lespez, L., Rasse, M., Camara, A., Mercier, N., Huysecom, É., 2017. Chronologie du Paléolithique ouest africain: premières datations OSL de la Vallée de la Falémé (Sénégal). L'Anthropologie 121 (1–2), 1–8.
Lioubine, V.P., Guédé, F.Y., 2000. The Palaeolithic of Republic Côte d'Ivoire (West Africa), vol. III. Russian Academy of Sciences, Institute of the History of Material Culture Proceedings, Saint Petersburg.
McBrearty, S., 1988. The Sangoan-Lupemban and Middle Stone Age sequence at the Muguruk site, western Kenya. World Archaeol. 19, 388–420.
McBrearty, S., Brooks, A.S., 2000. The revolution that wasn't: a new interpretation of the origin of modern human behavior. J. Hum. Evol. 39, 453–563.
McBrearty, S., Tryon, C., 2006. From Acheulean to Middle Stone Age in the Kapthurin formation, Kenya. In: Hovers, E., Kuhn, S. (Eds.), Transition Before the Transition. Springer, Boston, pp. 257–277.
Mercier, N., Falguères, C., 2007. Field gamma dose-rate measurement with a NaI (Tl) detector: re-evaluation of the "threshold" technique. Ancient TL 25, 1–4.
Metcalfe, C.R., 1960. Anatomy of the Monocotyledons, Lineae. Oxford University Press, London.
Metcalfe, C.R., 1971. Anatomy of the Monocotyledons, Cyperaceae, vol. 5. Clarendon Press, Oxford.
Michel, P., 1973. Les bassins des fleuves Sénégal et Gambie. Etude géomorphologique, vol. 63. Mémoire ORSTOM, Paris.
Morgan, L.E., Renne, P.R., 2008. Diachronous dawn of Africa's Middle Stone Age: new 40Ar/39Ar ages from the Ethiopian Rift. Geology 36, 967–970.
Mourre, V., 2003. Discoïde ou pas discoïde? Réflexions sur la pertinence des critères techniques définissant le débitage discoïde. BAR Int. Ser. 1120, 1–18.
Murray, A.S., Wintle, A.G., 2000. Luminescence dating of quartz using an improved single-aliquot regenerative-dose protocol. Radiat. Meas. 32, 57–73.
Murray, A.S., Wintle, A.G., 2003. The single aliquot regenerative dose protocol: potential for improvements in reliability. Radiat. Meas. 37 (4–5), 377–381.
Murungi, M.L., Bamford, M.K., 2020. Revised taxonomic interpretations of Cyperaceae phytoliths for (paleo) botanical studies with some notes on terminology. Rev. Palaeobot. Palynol. 275, 104–189.
Nathan, R.P., Mauz, B., 2008. On the dose-rate estimate of carbonate-rich sediments for trapped charge dating. Radiat. Meas. 43, 14–25.
Neumann, K., Fahmy, A., Lespez, L., Ballouche, A., Huysecom, E., 2009. The Early Holocene palaeoenvironment of Ounjougou (Mali): phytoliths in a multiproxy context. Palaeogeogr. Palaeoclimatol. Palaeoecol. 276, 87–106.
Neumann, K., Fahmy, A.G., Müller-Scheeßel, N., Schmidt, M., 2017. Taxonomic, ecological and palaeoecological significance of leaf phytoliths in West African grasses. Quat. Int. 434, 15–32.
Niang, K., Ndiaye, M., 2016. The Middle Palaeolithic of West Africa: Lithic techno-typological analyses of the site of Tiemassas, Senegal. Quat. Int. 408, 4–15.
Niang, K., Blinkhorn, J., Ndiaye, M., 2018. The oldest Stone Age occupation of coastal West Africa and its implications for modern human dispersals: New insight from Tiémassas. Quat. Sci. Rev. 188, 167–173.
Niang, K., Blinkhorn, J., Ndiaye, M., Bateman, M., Seck, B., Sawaré, G., 2020. The Middle Stone Age occupations of Tiémassas, coastal West Africa, between 62 and 25 thousand years ago. J. Archaeol. Sci. Rep. 34, 102658.
Novello, A., Barboni, D., Berti-Equille, L., Mazur, J.C., Poilecot, P., Vignaud, P., 2012. Phytolith signal of aquatic plants and soils in Chad, Central Africa. Rev. Palaeobot. Palynol. 178, 43–58.
Novello, A., Barboni, D., 2015. Grass inflorescence phytoliths of useful species and wild cereals from sub-Saharan Africa. J. Archaeol. Sci. 59, 10–22.
Novello, A., Lebatard, A.-E., Moussa, A., Barboni, D., Sylvestre, F., Bourles, D.L., Pailles, C., Buchet, G., Decarreau, A., Duringer, P., Ghienne, J.-F., Maley, J., Mazur, J.-C., Roquin, C., Schuster, M., Vignaud, P., 2015. Diatom, phytolith, and pollen records from a 10Be/9 Be dated lacustrine succession in the Chad basin: insight on the Miocene-Pliocene paleoenvironmental changes in Central Africa. Palaeogeogr. Palaeoclimatol. Palaeoecol. 430, 85–103.
Nygaard, S.E., Talbot, M.R., 1984. Stone Age archaeology and environment on the southern Accra plains, Ghana. Norweg. Archaeol. Rev. 17, 19–38.
Ollendorf, A.L., 1992. Toward a classification scheme of sedge (Cyperaceae) phytoliths. In: Rapp Jr., G., Mulholland, S.C. (Eds.), Phytolith Systematics: Emerging Issues. Plenum Press, New York, pp. 91–111.
Owen, W.E., 1938. The Kombewa culture, Kenya Colony. Man 38, 203–205.
Paradis, G., 1980. Découverte d'une industrie paléolithique d'âge « Sangoen » dans la Basse Côte d'Ivoire. Note de Paradis G. présentée par Théodore Monod. C. R. Acad. Sci Paris, Tome 290, 1393–1395.
Piperno, D.R., 2006. Phytoliths: A Comprehensive Guide for Archaeologists and Paleoecologists. AltaMira Press, Oxford.
Porraz, G., Parkington, J.E., Rigaud, J.P., Miller, C.E., Poggenpoel, C., Tribolo, C., Archer, W., Cartwright, C.R., Charrié-Duhaut, A., Dayet, L., Igreja, M., Mercier, N., Schmidt, P., Verna, C., Texier, P.-J., 2013. The MSA sequence of Diepkloof and the history of southern African Late Pleistocene populations. J. Archaeol. Sci. 40, 3542–3552.
Postek, M.T., 1981. The Occurrence of Silica in the Leaves of *Magnolia grandiflora* L. Bot. Gaz. 142, 124–134.
Prescott, J.R., Hutton, J.T., 1994. Cosmic ray contributions to dose rates for luminescence and ESR dating: large depths and long-term time variations. Radiat. Meas. 23 (2–3), 497–500.
Quickert, N.A., Godfrey-Smith, D.I., Casey, J.L., 2003. Optical and thermoluminescence dating of Middle Stone Age and Kintampo bearing sediments at Birimi, a multi-component archaeological site in Ghana. Quat. Sci. Rev. 22 (10–13), 1291–1297.
Rabett, R.J., 2018. The success of failed *Homo sapiens* dispersals out of Africa and into Asia. Nat. Ecol. Evol. 2, 212–219.
Radomski, K.U., Neumann, K., 2011. Grasses and grinding stones: inflorescence phytoliths from modern West African Poaceae and archaeological atone artefacts. In: Fahmy, A.G., Kahlheber, S., D'Andrea, A.C. (Eds.), Windows on the African Past. Current Approaches to African Archaeobotany. Africa Magna Verlag, Frankfurt am Main, pp. 153–166.
Rasse, M., Tribolo, C., Soriano, S., Huysecom, E., 2012. Premières données chronostratigraphiques sur les formations du Pléistocène supérieur de la «falaise» de Bandiagara (Mali, Afrique de l'Ouest). Quaternaire 23, 5–23.
Rasse, M., Lespez, L., Lebrun, B., Tribolo, C., Chevrier, B., Douze, K., Garnier, A., Davidoux, S., Hajdas, I., Ollier, C., Ndiaye, M., Camara, A., Huysecom, E., 2020. Morpho-sedimentary synthesis and archaeological occurrences in the Falémé Valley (80-5 ka; east Senegal): continuing occupations during the Pleistocene-Holocene transition. Quaternaire 31, 71–88.
Richter, D., Grün, R., Joannes-Boyau, R., Steele, T.E., Amani, F., Rué, M., Fernandes, P., Raynal, J.-P., Geraads, D., Ben-Ncer, A., Hublin, J.-J., McPherron, S.P., 2017. The age of the hominin fossils from Jebel Irhoud, Morocco, and the origins of the Middle Stone Age. Nature 546, 293–296.
Roberts, R.G., Galbraith, R.F., Yoshida, H., Laslett, G.M., Olley, J.M., 2000. Distinguishing dose populations in sediment mixtures: a test of single-grain optical dating procedures using mixtures of laboratory-dosed quartz. Radiat. Meas. 32 (5–6), 459–465.
Runge, F., 1999. The opal phytolith inventory of soils in central Africa–quantities, shapes, classification, and spectra. Rev. Palaeobot. Palynol. 107, 23–53.
Sahle, Y., Beyene, Y., Defleur, A., Asfaw, B., WoldeGabriel, G., Hart, W.K., Morgan, L.E., Renne, P.R., Carlson, J., White, T.D., 2019. Revisiting Herto: new evidence of *Homo sapiens* from Ethiopia. In: Sahle, Y., Reyes-Centeno, H., Bentz, C. (Eds.), Modern Human Origins and Dispersal. Kerns Verlag Tübingen, Tübingen, pp. 73–104.
Scerri, E.M., 2017. The North African Middle Stone Age and its place in recent human evolution. Evol. Anthropol. 26, 119–135.
Scerri, E.M., Blinkhorn, J., Groucutt, H.S., Niang, K., 2016. The Middle Stone Age archaeology of the Senegal river valley. Quat. Int. 408, 16–32.
Scerri, E.M., Blinkhorn, J., Niang, K., Bateman, M.D., Groucutt, H.S., 2017. Persistence of Middle Stone Age technology to the Pleistocene/Holocene transition supports a complex hominin evolutionary scenario in West Africa. J. Archaeol. Sci. Rep. 11, 639–646.
Scerri, E.M., Thomas, M.G., Manica, A., Gunz, P., Stock, J.T., Stringer, C., Grove, M., Groucutt, H.S., Timmermann, A., Rightmire, G.P., d'Errico, F., Tryon, C.A., Drake, N.A., Brooks, A.S., Dennell, R.W., Durbin, R., Henn, B.M., Lee-Thorp, J., deMenocal, P., Petraglia, M.D., Thompson, J.C., Scally, A., Chikhi, L., 2018. Did our species evolve in subdivided populations across Africa, and why does it matter? Trends Ecol. Evol. 33, 582–594.
Scerri, E.M., Niang, K., Candy, I., Blinkhorn, J., Mills, W., Cerasoni, J.N., Bateman, M.D., Crowther, A., Groucutt, H.S., 2021. Continuity of the Middle Stone Age into the Holocene. Sci. Rep. 11 (70).
Sheppard, P.J., Kleindienst, M.R., 1996. Technological change in the Earlier and Middle Stone Age of Kalambo Falls (Zambia). Afr. Archaeol. Rev. 13, 171–196.
Soper, R.C., 1965. The Stone Age in Northern Nigeria. J. Hist. Soc. Niger. 3, 175–194.
Soriano, S., 2003. Quand archaïque n'est pas ancien! Étude de cas dans le Paléolithique du Pays dogon (Ounjougou, Mali). Annales de la Fondation Fyssen 18, 79–92.
Soriano, S., Rasse, M., Tribolo, C., Huysecom, E., 2010. Ounjougou: a long Middle Stone Age sequence in the Dogon country (Mali). In: Allsworth-Jones, P. (Ed.), West African Archaeology. New Developments, New Perspectives. Archaeopress, Oxford, pp. 1–14.
Stewart, M., Clark-Wilson, R., Breeze, P.S., Janulis, K., Candy, I., Armitage, S.J., Ryves, D.B., Louys, J., Duval, M., Price, G.J., Cuthbertson, P., Bernal, M.A., Drake, N.A., Alsharekh, A.M., Zahrani, B., Al-Omari, A., Roberts, P., Groucutt, H.S., Petraglia, M.D., 2020. Human footprints provide snapshot of last interglacial ecology in the Arabian interior. Sci. Adv. 6 (38), eaba8940.
Strömberg, C.A., 2004. Using phytolith assemblages to reconstruct the origin and spread of grass-dominated habitats in the great plains of North America during the late Eocene to early Miocene. Palaeogeogr. Palaeoclimatol. Palaeoecol. 207 (3–4), 239–275.
Taylor, N., 2016. Across rainforests and woodlands: a systematic reappraisal of the Lupemban Middle Stone Age in Central Africa. In: Jones, S.C., Stewart, B.A. (Eds.), Africa from MIS 6-2. Springer, Dordrecht, pp. 273–299.
Thévéniaut, H., Ndiaye, P.M., Buscail, F., Coueffe, R., Delor, C., Fullgraf, T., Goujou, J.-C., 2010. Notice Explicative de la Carte Géologique du Sénégal Oriental au 1/500000e. Ministère des Mines, de l'Industrie, de l'Agro-Industrie et des PME. Direction des Mines et de la Géologie, Dakar.
Thomsen, K.J., Murray, A.S., Buylaert, J.P., Jain, M., Hansen, J.H., Aubry, T., 2016. Testing single-grain quartz OSL methods using sediment samples with independent age control from the Bordes-Fitte rockshelter (Roches d'Abilly site, Central France). Quat. Geochronol. 31, 77–96.

Tribolo, C., Rasse, M., Soriano, S., Huysecom, E., 2015. Defining a chronological framework for the Middle Stone Age in West Africa: comparison of methods and models for OSL ages at Ounjougou (Mali). Quat. Geochronol. 29, 80–96.
Tryon, C.A., Faith, J.T., 2013. Variability in the middle stone age of eastern Africa. Curr. Anthropol. 54, S234–S254.
Van Peer, P., Fullagar, R., Stokes, S., Bailey, R.M., Moeyersons, J., Steenhoudt, F., Geerts, A., Vanderbeken, T., De Dapper, M., Geus, F., 2003. The Early to Middle Stone Age transition and the emergence of modern human behaviour at site 8-B-11, Sai Island, Sudan. J. Hum. Evol. 45, 187–193.
Weldeab, S., Lea, D.W., Schneider, R.R., Andersen, N., 2007. 155,000 years of West African monsoon and ocean thermal evolution. Science 316, 1303–1307.
Wendorf, F., Schild, R., 1974. A Middle Stone Age Sequence from the central Rift Valley, Ethiopia. Polska Akademia Nauk, Wroclaw.
White, F., 1983. The vegetation map of Africa. UNESCO, Paris.
Wilkins, J., Schoville, B.J., Brown, K.S., Chazan, M., 2012. Evidence for early hafted hunting technology. Science 338, 942–946.
Will, M., Conard, N.J., Tryon, C.A., 2019. Timing and trajectory of cultural evolution on the African continent during 300–40 ka. In: Sahle, Y., Reyes-Centeno, H., Bentz, C. (Eds.), Modern Human Origins and Dispersal. Rern Verlag, Tübingen, pp. 25–72.
Wintle, A.G., Murray, A.S., 2006. A review of quartz optically stimulated luminescence characteristics and their relevance in single-aliquot regeneration dating protocols. Radiat. Meas. 41, 369–391.
Wurz, S., 2013. Technological trends in the Middle Stone Age of South Africa between MIS 7 and MIS 3. Curr. Anthropol. 54, S305–S319.